PLOS GENETICS
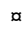
RESEARCH ARTICLE

Trehalose and α-glucan mediate distinct abiotic stress responses in *Pseudomonas aeruginosa*

Stuart D. Woodcock[1]⊙, Karl Syson[2]⊙, Richard H. Little[1], Danny Ward[1], Despoina Sifouna[3], James K. M. Brown[4], Stephen Bornemann[2]¤, Jacob G. Malone[1,3]*

1 Department of Molecular Microbiology, John Innes Centre, Norwich, United Kingdom, **2** Department of Biological Chemistry, John Innes Centre, Norwich, United Kingdom, **3** School of Biological Sciences, University of East Anglia, Norwich, United Kingdom, **4** Department of Crop Genetics, John Innes Centre, Norwich, United Kingdom

⊙ These authors contributed equally to this work.
¤ Current address: The Sainsbury Laboratory, Norwich Research Park, Norwich, United Kingdom
* jacob.malone@jic.ac.uk

Abstract

An important prelude to bacterial infection is the ability of a pathogen to survive independently of the host and to withstand environmental stress. The compatible solute trehalose has previously been connected with diverse abiotic stress tolerances, particularly osmotic shock. In this study, we combine molecular biology and biochemistry to dissect the trehalose metabolic network in the opportunistic human pathogen *Pseudomonas aeruginosa* PAO1 and define its role in abiotic stress protection. We show that trehalose metabolism in PAO1 is integrated with the biosynthesis of branched α-glucan (glycogen), with mutants in either biosynthetic pathway significantly compromised for survival on abiotic surfaces. While both trehalose and α-glucan are important for abiotic stress tolerance, we show they counter distinct stresses. Trehalose is important for the PAO1 osmotic stress response, with trehalose synthesis mutants displaying severely compromised growth in elevated salt conditions. However, trehalose does not contribute directly to the PAO1 desiccation response. Rather, desiccation tolerance is mediated directly by GlgE-derived α-glucan, with deletion of the *glgE* synthase gene compromising PAO1 survival in low humidity but having little effect on osmotic sensitivity. Desiccation tolerance is independent of trehalose concentration, marking a clear distinction between the roles of these two molecules in mediating responses to abiotic stress.

Author summary

To survive outside their host, pathogenic bacteria must withstand various environmental stresses. The sugar molecule trehalose is associated with a range of abiotic stress tolerances, particularly osmotic shock. In this study, we analyse the trehalose metabolic network in the human pathogen *Pseudomonas aeruginosa* PAO1 and define its role in abiotic

stress protection. We show that trehalose metabolism in PAO1 is intimately connected to the biosynthesis of branched α-glucan, or glycogen. Disruption of either trehalose or glycogen biosynthesis significantly reduces the ability of PAO1 to survive on steel work surfaces. While both trehalose and glycogen are important for stress tolerance, they counter very different stresses. Trehalose is important for the osmotic stress response, and survival in conditions of elevated salt. On the other hand, glycogen is responsible for desiccation tolerance and survival in low humidity environments. Trehalose does not apparently contribute to desiccation tolerance, marking a clear distinction between the roles of trehalose and glycogen in mediating abiotic stress responses in *P. aeruginosa*.

Introduction

Pseudomonas aeruginosa is a significant human pathogen and one of the most common causes of nosocomial infections [1]. It is considered a serious medical threat, on a par with methicillin-resistant *Staphylococcus aureus* and extensively drug-resistant *Mycobacterium tuberculosis* [2]. *P. aeruginosa* is an opportunistic pathogen that primarily affects immunocompromised individuals, including patients with immunodeficiencies [3], burn or major injury victims [4] and cannula or catheter implant patients [5]. It is also a major pneumonia agent, causing both acute and chronic lung infections. Acute infections typically arise following trauma and can be difficult to eradicate due to a high level of intrinsic antibiotic resistance [6]. Chronic infections often result from a failure to resolve acute infection and involve the persistent, long-term colonisation of the patient [7]. Chronic *P. aeruginosa* infections occur in 80% of adult cystic fibrosis (CF) patients and significantly increase morbidity and mortality compared to uninfected CF patients [7, 8]. The difficulty of treating established *P. aeruginosa* infections means that considerable effort is directed towards the prevention of chronic infection in the first place [9].

Throughout its lifecycle *P. aeruginosa* is exposed to diverse environmental challenges, both in association with its hosts and in the wider environment. Outside of an infection, it is subject to frequent changes in temperature, pH, ultra-violet radiation, salinity, humidity, and nutrient availability [10, 11]. Similarly, during colonisation of the CF lung *P. aeruginosa* is exposed to various abiotic stresses, including nutrient starvation, oxidative stress and desiccation [12]. Similar to other bacteria, *P. aeruginosa* responds to abiotic stresses using a variety of mechanisms, including the formation of biofilms [13], reduction or redirection of metabolic pathways [14], regulation of lipopolysaccharides [15] or stress response proteins [16] and the production of protective solutes [17]. Understanding the mechanisms and pathways *P. aeruginosa* uses to survive abiotic stresses is crucial to reduce and restrict environmental sources of these pathogenic bacteria.

Trehalose is a ubiquitous disaccharide found in virtually all organisms [18] and implicated in diverse stress responses, most notably osmotic stress [19, 20]. In bacteria, trehalose has also been implicated in protection from desiccation stress [21–23], the development of nitrogen-fixing root nodules [23], oxidative stress protection [24] and facilitating bacterial infection in *Mycobacterium tuberculosis* [25, 26] and *Xanthomonas citri* [27]. Exogenous addition of trehalose has been shown to protect *Pseudomonas putida* from entering a desiccation-induced, non-viable state [28]. There are three widespread trehalose metabolic pathways in bacteria [29]. The OtsA/B pathway produces trehalose from glucose 6-phosphate and UDP-glucose via a trehalose-6-phosphate intermediate [30]. A standalone synthase TreS can produce trehalose through the isomerisation of maltose in some metabolic contexts [31, 32]. Finally, the TreY/TreZ pathway produces trehalose by isomerising and hydrolysing α-glucan [33]. Different

bacterial species contain varying combinations of all three pathways [34], with most *Pseudomonas* spp. missing OtsA/B, but encoding TreS and TreY/Z.

Bacterial glycogen is a large α-glucan polysaccharide formed from thousands of glucose monomers with α-1,4 glycosidic links and α-1,6 linked branch points [35]. This α-glucan functions as a ubiquitous carbon store, which accumulates during exponential bacterial growth and can be recycled when necessary. It also acts as a virulence factor of *Mycobacterium tuberculosis* [36, 37]. There are two main α-glucan biosynthetic pathways in bacteria. In the classical GlgC-GlgA pathway [38], GlgC generates ADP-glucose from glucose 1-phosphate (G1P) [39, 40]. ADP-glucose is then used by GlgA to extend an α-1,4 linked α-glucan chain [41, 42], with branches being added by GlgB [43, 44]. GlgX and GlgP break down α-glucan by debranching [45] and removing glucose units from the non-reducing end of the glucan [46], respectively. More recently, the alternative GlgE pathway was discovered in *M. tuberculosis* [26, 47] and subsequently found to be encoded in 14% of sequenced bacterial genomes [48]. This pathway employs four enzymes; TreS, Pep2, GlgE and GlgB to produce branched α-glucan from trehalose via maltose and maltose-1-phosphate (M1P) [47], thus making a direct metabolic link between trehalose and α-glucan.

The production and roles of trehalose and α-glucan are currently poorly understood in *Pseudomonas*, with relatively few studies of trehalose biosynthesis [49–52] and little knowledge of the role of α-glucan. Mucoid *P. aeruginosa* isolates, which evolve during chronic CF lung infection, show marked differences in osmoprotectant accumulation from planktonic isolates, with an apparent switch from glycine–betaine to trehalose utilisation accompanying the visible alginate overproduction phenotype [52]. Perhaps related to this, long-term *P. aeruginosa* CF lung isolates show a significantly reduced tendency to utilize exogenous trehalose as a carbon source compared to more recent infections [53]. Recently, deletions of the *treS* and *treY/Z* loci in *P. aeruginosa* PA14 were shown to abolish trehalose production and attenuate model plant infection [50] implicating trehalose as a stress protectant and possible virulence factor. Similarly, trehalose-related gene disruption in *P. syringae* pv. *tomato* resulted in osmotic sensitivity and strains attenuated in plant infection [49]. However, given the potential intrinsic biochemical connections between trehalose and α-glucan biosynthesis, the physiological roles of each molecule in *P. aeruginosa* are currently unclear.

To address this, we fully characterised the trehalose and α-glucan biosynthetic pathways of *P. aeruginosa* to establish how they were configured. We then determined their physiological functions and contribution to abiotic stress tolerance and survival in challenging environments. We demonstrate that contrary to current models, trehalose plays no appreciable role in adapting bacteria to desiccation stress. Rather, this phenotype is mediated in large part by the accumulation of α-glucan. Disruption of either trehalose or branched α-glucan production significantly compromised the ability of *P. aeruginosa* to survive on metal work surfaces, suggesting that abiotic survival in the environment requires the interplay of both stress tolerance phenotypes.

Results

Bioinformatic prediction of the trehalose/α-glucan biosynthetic pathway

In *P. aeruginosa* PAO1, the genes associated with trehalose/α-glucan biosynthesis are found in two predicted operons (Fig 1A) [50, 54]. The predicted functions of the genes are summarised in Table 1. The first cluster consists of three genes, *glgE*, *treS* and *glgB*, that collectively code for the GlgE α-glucan biosynthetic pathway. The predicted *treS* gene is fused to the predicted maltokinase gene *pep2*, as is most often the case in bacteria containing the GlgE pathway [48], and is henceforth referred to as *treS/pep2*. The second cluster encodes classical α-glucan metabolic
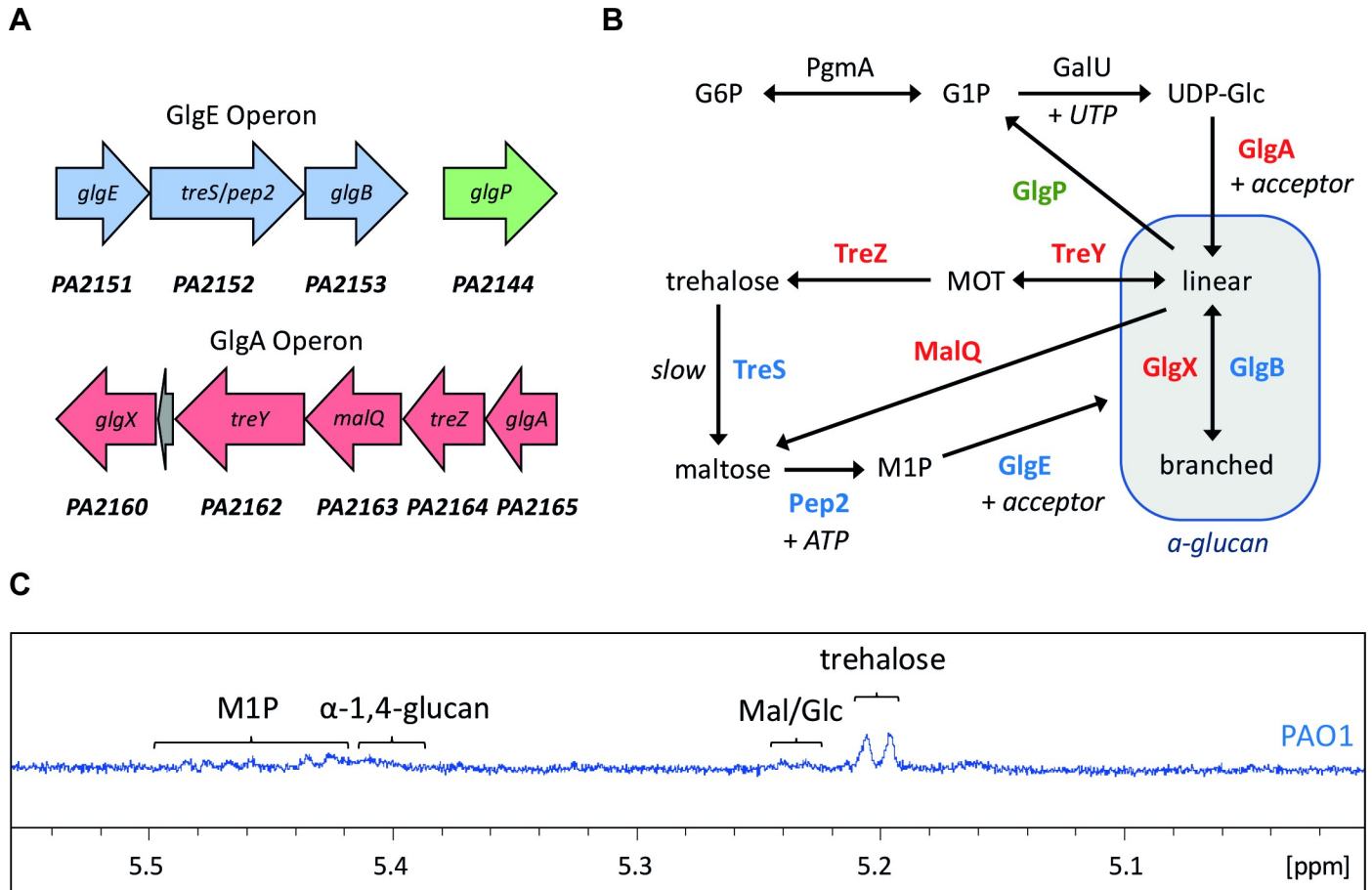
A

Fig 1. A) PAO1 trehalose/α-glucan biosynthetic genes cluster in two predicted operons, while the *glgP* gene is orphaned. Rightward pointing arrows indicate genes on the positive strand, and leftward indicates the negative strand. **B) Model for trehalose and α-glucan biosynthesis in PAO1.** The colours of the protein names correspond to the operons shown in 1A. Arrows indicate the primary direction of flux between substrates. Abbreviations are used as follows: G6P –glucose-6-phosphate, G1P –glucose-1-phosphate, UDP-Glc–UDP-glucose, MOT–maltooligosyltrehalose, M1P –maltose-1-phosphate. **C)** **¹H-NMR spectrum for PAO1.** Peaks corresponding to key metabolites are indicated. Mal/Glc–maltose/glucose.

https://doi.org/10.1371/journal.pgen.1009524.g001

Table 1. Predicted functions of the trehalose/α-glucan metabolic genes in *P. aeruginosa* PAO1 that were tested in this study.

Gene name	Gene number	Predicted enzyme function	Reaction catalysed	EC number
glgE	PA2151	Maltosyltransferase	Extension of α-glucan using M1P as the donor	2.4.99.16
treS/ pep2	PA2152	Trehalose-maltose isomerase/ maltokinase	Isomerisation between trehalose and maltose/phosphorylation of maltose to M1P using ATP	5.4.99.16/ 2.7.1.175
glgB	PA2153	Glycogen branching enzyme	Introduction of α-1,6-linked branches into α-glucan	2.4.1.18
glgA	PA2165	Glycogen synthase	Extension of α-glucan using UDP-glucose as the donor	2.4.1.11
treZ	PA2164	Maltooligosyltrehalose hydrolase	Hydrolysis of maltooligosyltrehalose to liberate trehalose	3.2.1.141
malQ	PA2163	α-Glucanotransferase	Disproportionation of linear maltooligosaccharides with degrees of polymerisation of ≥ 2	2.4.1.25
treY	PA2162	Maltooligosyltrehalose synthase	Conversion of reducing end terminal α-1,4 linkage into an α-1,α-1 linkage, forming maltooligosyltrehalose	5.4.99.15
glgX	PA2160	Glycogen debranching enzyme	Hydrolysis of α-1,6 linkages of branched α-glucan	3.2.1.196
glgP	PA2144	Glycogen phosphorylase	Degradation of non-reducing ends of α-glucan yielding glucose 1-phosphate	2.4.1.1

https://doi.org/10.1371/journal.pgen.1009524.t001

enzymes [48], consisting of *glgA*, *treZ*, the glucanotransferase gene *malQ* [49], *treY* and *glgX*. The gene for the recycling enzyme GlgP is orphaned and found elsewhere in the genome. In common with other pseudomonads, *P. aeruginosa* does not contain the *otsA/otsB* trehalose synthesis pathway genes [49].

By combining earlier predictions for trehalose biosynthesis in *Pseudomonas* [49, 50] with the known metabolic GlgE pathways in actinomycetes, we produced a model for trehalose/α-glucan biosynthesis in *P. aeruginosa* (Fig 1B). The clustering of genes within the *glgA* operon suggests it functions to produce trehalose from GlgA-derived linear α-glucan, as previously described [49, 50]. Conversely, the genomic clustering of the four GlgE pathway genes (*glgE*, *treS/pep2* and *glgB*) implies a role for this operon in the conversion of trehalose into branched α-glucan, contrary to previous assumptions in pseudomonads. Although PAO1 also contains genes for the phosphoglucomutase PgmA and the UDP-glucose pyrophosphorylase GalU, the ADP-glucose phosphorylase gene *glgC* is not present. This suggests that *P. aeruginosa* uses the activated sugar UDP-glucose as the initial substrate for trehalose/α-glucan biosynthesis [37]. This contrasts with *M. tuberculosis* and most other bacteria that use primarily ADP-glucose [37, 48].

PAO1 produces α-glucan, trehalose and M1P

To determine the levels of key metabolites in PAO1, the metabolome of the wild-type strain was extracted after growth in M9 medium and analysed using ^{1}H-NMR spectroscopy. Wild-type PAO1 accumulated trehalose and M1P to 0.13 ± 0.03 and $0.30 \pm 0.03\%$ of the cellular dry weight, respectively. *Pseudomonas* spp. are known to accumulate significantly less α-glucan than other bacteria, with previous studies reporting no detectable α-glucan accumulation for PA14 or *P. syringae Pto* [50, 55]. However, we detected a broad peak corresponding to α-1,4-linkages at 5.41 ppm in the NMR spectrum, consistent with the accumulation of high molecular weight α-glucan in PAO1 (Fig 1C). Additional evidence for the production of α-glucan is described below. The detection of signals for trehalose, M1P and α-glucan suggests that the GlgE pathway is present and functional in PAO1.

To experimentally test the model in Fig 1B, in-frame deletions were produced for each of the predicted trehalose/α-glucan biosynthesis genes in PAO1, as well as selected multiple gene deletions. The effect of each gene deletion on the bacterial soluble metabolome was then determined using ^{1}H-NMR spectroscopy. The relative accumulations of trehalose and M1P for the tested mutants are summarised in Table 2, with selected NMR spectra shown in **S1 Fig**. The qualitative presence or absence of α-glucan was evident, but quantitation was precluded due to the breadth of the signal. In addition, it was not possible to distinguish glucose and maltose because their α-anomeric signals overlapped, and other distinguishing signals were hidden by signals from other metabolites.

GlgA and GlgP produce and degrade α-glucan chains, respectively

GlgA is annotated as a glycogen synthase [56] and is predicted to be the first committed enzyme in our metabolic model. GlgA is a Glycosyl Transferase 5 family member and is expected to extend linear α-glucan (i.e. maltooligosaccharides) and possibly branched α-glucan using UDP-glucose as the donor substrate. As predicted, deletion of *glgA* led to the complete loss of downstream metabolites in PAO1 (Table 2). To further test the activity of GlgA, the recombinant protein's capacity to utilise UDP-glucose was tested *in vitro* using MALDI mass spectrometry. GlgA was able to produce linear α-glucan from UDP-glucose without the addition of an acceptor maltooligosaccharide (Fig 2A). In addition, the production of α-1,4 linkages was confirmed using NMR spectroscopy with a doublet resonance at 5.32 ppm at the

Table 2. Accumulation of trehalose and M1P in PAO1 strains.

Strain	Trehalose (%)	M1P (%)	Presence of α-glucan
PAO1	0.13 ± 0.03	0.30 ± 0.03	+
PAO1 Δ*glgE*	0.12 ± 0.05	2.35 ± 0.43*	++
PAO1 Δ*treS/pep2*	0.89 ± 0.25*	-	-
PAO1 Δ*glgB*	0.74 ± 0.08*	0.78 ± 0.04*	++[a]
PAO1 Δ*glgA*	-	-	-
PAO1 Δ*treZ*	-	0.25 ± 0.06	++
PAO1 Δ*malQ*	0.32 ± 0.04*	0.22 ± 0.03	++
PAO1 Δ*treY*	-	0.45 ± 0.13	+
PAO1 Δ*glgX*	-	0.03 ± 0.03*	-
PAO1 Δ*glgP*	0.24 ± 0.01*	0.29 ± 0.09	+
PAO1:: *otsA/otsB*	0.17 ± 0.06	0.17 ± 0.02*	+
Δ*treS/pep2*:: *otsA/otsB*	0.91 ± 0.13*	-	-
Δ*glgA*:: *otsA/otsB*	0.06 ± 0.03*	0.48 ± 0.06*	+
Δ*glgA* Δ*glgE*:: *otsA/otsB*	0.07 ± 0.02	0.66 ± 0.11*	-
PAO1 *[liquid]*	0.08 ± 0.02	-	+
PAO1 *[liquid + NaCl]*	3.66 ± 1.11*	-	-

Values are percentages of cellular dry weight ± standard error.–indicates no metabolite detected

* indicates significant differences compared to the wild-type PAO1 as determined by a student's t-test (p ≤ 0.05, 2-tailed, equal variance).

Presence or absence of α-glucan as indicated by + or–respectively, where ++ indicates increased α-glucan production compared with the wild-type strain, [a] indicates linear α-glucan only, [liquid] indicates cells grown in liquid M9 media.

expense of the donor resonances. The most likely priming mechanism involves the slow initial hydrolysis of each NDP-glucose to yield glucose that can subsequently act as the initial acceptor substrate. The highest polymerase activity was with UDP-glucose, as expected given the lack of the *glgC* gene coding for the enzyme responsible for the production of ADP-glucose in *Pseudomonas spp*. GlgA is therefore a UDP-glucose-dependent glycogen synthase whose absence leads to the loss of all trehalose/α-glucan metabolites in PAO1.

Our model suggests that the glycogen phosphorylase GlgP degrades the non-reducing ends of α-glucan into glucose 1-phosphate (G1P). Deletion of *glgP* should therefore result in a higher accumulation of α-glucan and potentially trehalose and M1P. Based on examination of NMR spectra, the level of α-glucan appeared to increase relative to wild-type, although this response could not be quantified. In addition, the level of trehalose increased approximately 2-fold in the Δ*glgP* mutant, although the amount of M1P did not change significantly (Table 2). To confirm the phosphorylase activity of GlgP, the recombinant protein was incubated with maltohexaose in the presence of inorganic phosphate. NMR spectroscopy showed the expected production of α-glucose-1-phosphate by the appearance of a diagnostic resonance at 5.36 ppm (Fig 2B). The concentration of reducing ends remained constant, showing that GlgP does not hydrolyse α-1,4 linkages. Thus, GlgP is a glycogen phosphorylase whose absence leads to the increased accumulation of trehalose and α-glucan *in vivo*.

TreS/Pep2 converts trehalose into maltose-1-phosphate via maltose

Although TreS is commonly annotated as trehalose synthase, net flux through the enzyme will depend on its metabolic context. In the presence of the other GlgE pathway enzymes, flux is predicted to run in the direction of M1P and ultimately branched α-glucan. Such flux is driven by the strongly favourable free energies of the Pep2 maltokinase and branching enzyme
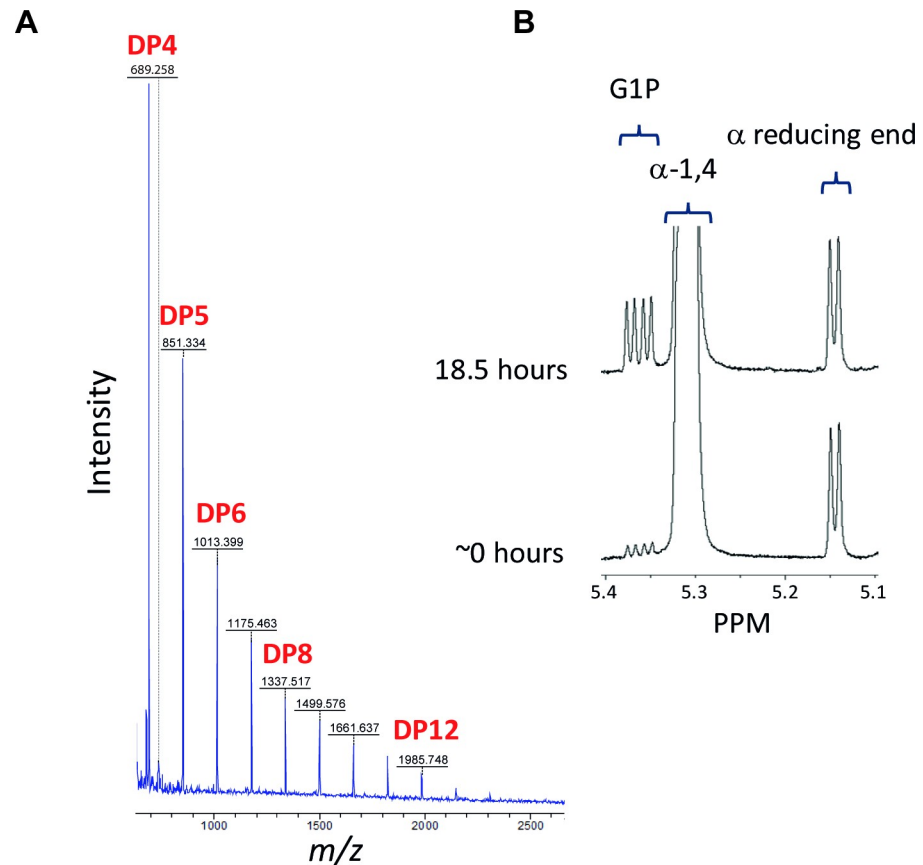
Fig 2. A) PAO1 GlgA converts UDP-glucose into maltooligosaccharides. GlgA was incubated with UDP-glucose and the resulting product mixture was analysed using MALDI mass spectrometry. The degree of polymerisation (DP) of the maltooligosaccharide products formed is indicated. **B) PAO1 GlgP is a phosphorylase.** GlgP was incubated with maltohexaose in the presence of inorganic phosphate. The appearance on a ^{1}H-NMR spectrum of an anomeric double-doublet resonance at 5.36 ppm is diagnostic of α-glucose-1-phosphate. The shortened maltooligosaccharide co-products maintain the reducing end of the substrate.

https://doi.org/10.1371/journal.pgen.1009524.g002

reactions, regardless of whether in an *in vitro* [57] or *in vivo* setting [32]. Thus, we predict that the TreS domain of the TreS/Pep2 fusion protein converts trehalose into maltose and the Pep2 domain converts maltose into M1P, driven by the free energy of ATP hydrolysis. Deletion of *treS/pep2* should result in an increased level of trehalose and the loss of M1P and other downstream metabolites. As predicted, analysis of the PAO1 Δ*treS/pep2* metabolome revealed an approximate 7–fold accumulation of trehalose compared to wild-type (Table 2), alongside the complete loss of M1P and α-glucan. This is fully consistent with TreS/Pep2 converting trehalose into M1P *via* maltose in PAO1.

Recombinant TreS/Pep2 exhibited trehalose synthase and maltokinase activity *in vitro*. Using a coupled assay detecting the co-production of ADP from the Pep2 reaction, activity was detected using either trehalose or maltose as the initial substrate. The pH optimum of the Pep2 maltokinase reaction with trehalose was 8 (Fig 3A). The rate of this activity increased linearly ~2-fold as a function of temperature between 25 and 50˚C (Fig 3B). The maltokinase activity conformed to a random order ternary complex mechanism (Fig 3C), with k_{cat} of 43.4 ± 1.5 s^{-1}, K_m^{ATP} 0.14 ± 0.01 mM, K_m^{Mal} 0.84 ± 0.08 mM, K_i^{ATP} 0.089 ± 0.021 mM and K_i^{Mal} 0.55 ± 0.13 mM. The activity of the TreS domain was confirmed by observing the equilibration of trehalose-maltose interconversion by NMR spectroscopy when the enzyme was
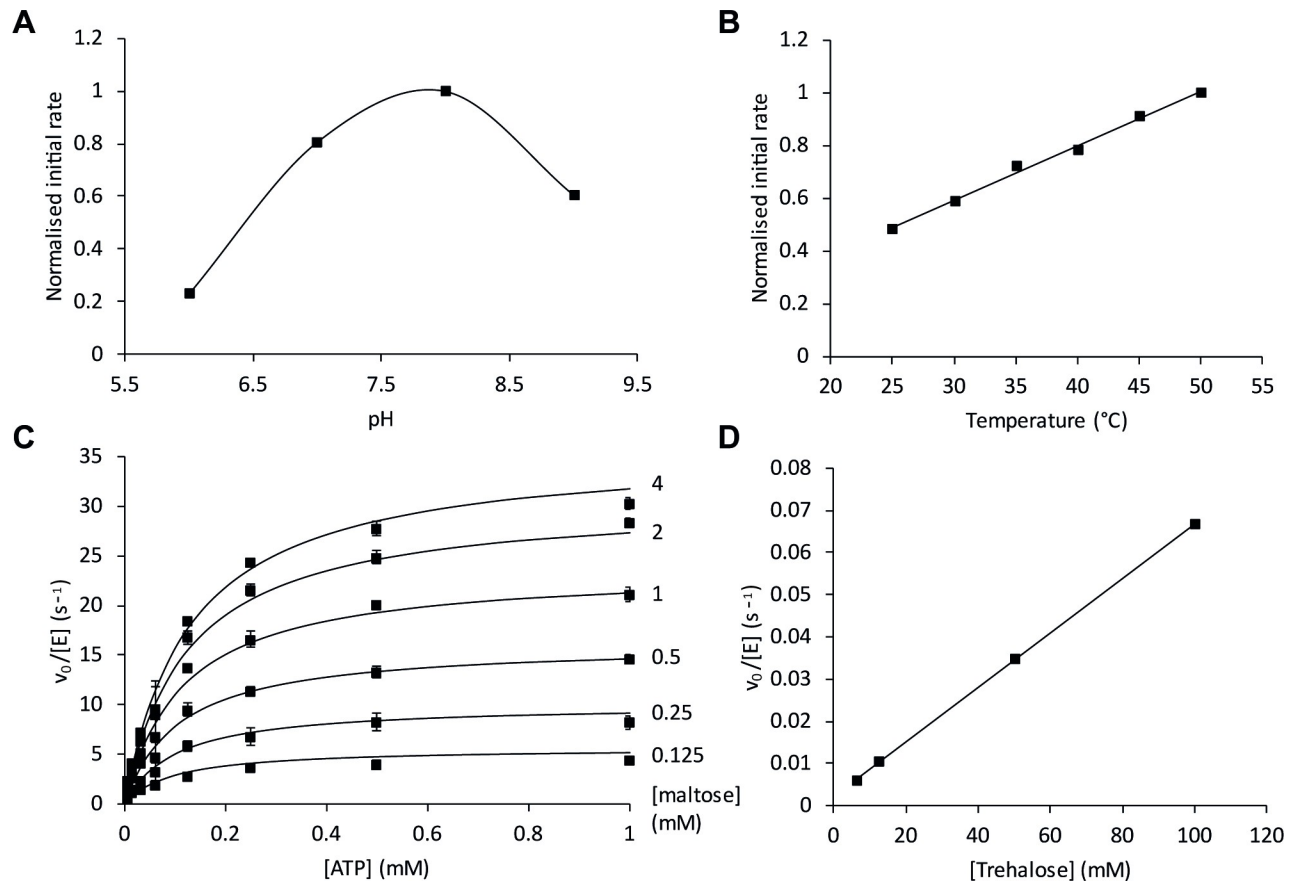
Fig 3. A-C) Dependence of PAO1 TreS/Pep2 maltokinase activity on pH, temperature, and substrate concentrations. Maltokinase activity was monitored by detecting the production of ADP using a coupled assay with maltose, phosphoenol pyruvate, pyruvate kinase, lactate dehydrogenase and NADH. **A)** Maltokinase activity of TreS/Pep2 with maltose and ATP was optimal at pH 8. **B)** Maltokinase activity increased ~2-fold linearly with temperature between 25 and 50˚C. Data points in A) and B) represent means of duplicate experiments. **C)** The maltokinase activity of TreS/Pep2 was determined as a function of ATP concentration with a series of fixed maltose concentrations. The smooth lines represent the fit to the data of a random order ternary complex mechanism. Data points show means of triplicate measurements and standard error. **D) The activity of TreS with trehalose** was monitored indirectly by detecting ADP production by Pep2 in a coupled reaction. The K_m for trehalose was evidently > 100 mM.

exposed to either trehalose or maltose (5 mM) as the initial substrate. The kinetics of the TreS activity with trehalose was tested by coupling it to the maltokinase assay. This showed that the activity of TreS was potentially rate-limiting with a high K_m for trehalose (> 100 mM), giving a k_{cat}/K_m of only 0.65 s^{-1} M^{-1} according to the initial slope of an initial rate vs trehalose concentration plot (Fig 3D). This is at the lower extremity of physiological relevance, but activity i*n vivo* could be higher in a cellular context.

GlgE extends α-glucan with M1P

The maltosyltransferase GlgE is predicted to extend α-glucan using M1P as a substrate (Fig 1). Deletion of *glgE* should result in the accumulation of M1P and other up-stream metabolites. As predicted, the M1P level increased almost 8-fold to 2.35 ± 0.43% of the cellular dry weight of the PAO1 Δ*glgE* mutant strain (Table 2). The up-stream metabolites maltose and/or glucose were also detected (not shown), and the (GlgA-derived) α-glucan level also appeared to increase.

Recombinant GlgE extended maltooligosaccharides *in vitro* with the donor M1P, releasing inorganic phosphate. The temperature and pH optima of the enzyme were 30˚C and 7,
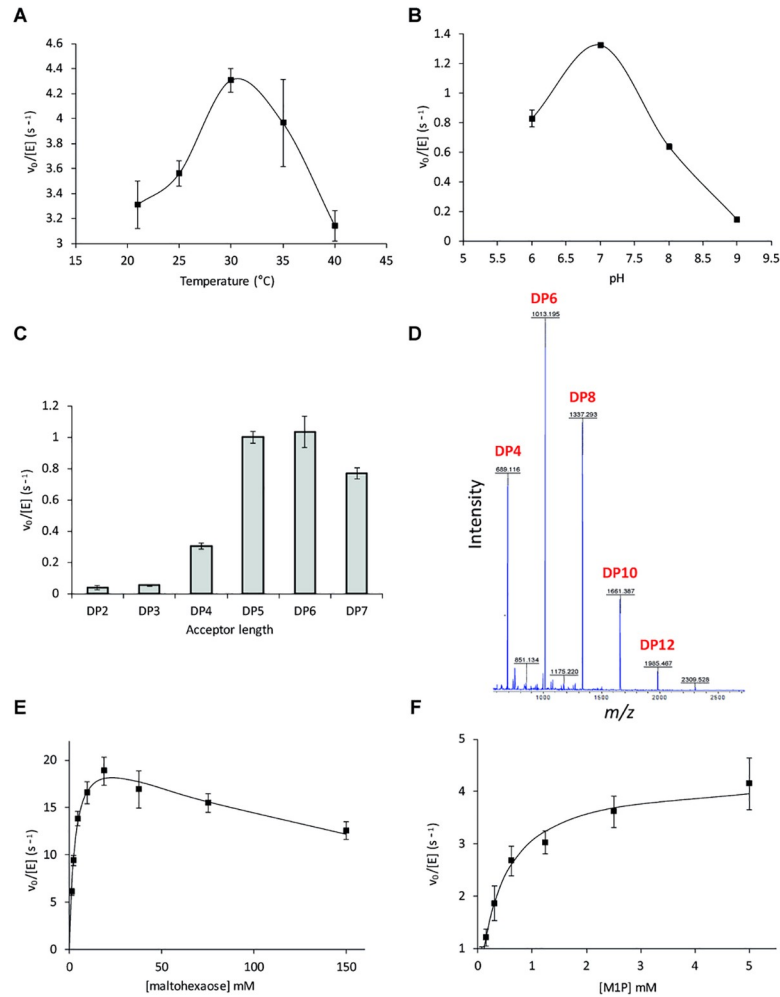
Fig 4. A-C) Dependence of PAO1 GlgE activity on pH, temperature, and acceptor chain length. GlgE activity with M1P and an acceptor was monitored by detecting the release of inorganic phosphate in a stopped assay. **A)** The temperature optimum of GlgE activity with maltohexaose was 30°C. **B)** The pH optimum of GlgE activity with maltohexaose was 7. **C)** GlgE preferentially extends linear maltooligosaccharides with a DP of 5 to 7. All data points represent means of triplicate measurements and standard errors. **D) PAO1 GlgE exhibits disproportionation activity.** GlgE was incubated with maltohexaose and the resulting product mixture was analysed using MALDI mass spectrometry. The DP of the maltooligosaccharide products formed is indicated. Note that GlgE transfers maltose groups between maltooligosaccharides. **E-F) The kinetics of the PAO1 GlgE-catalysed maltohexaose extension by M1P. E)** GlgE activity was determined as a function of maltohexaose concentration using 1 mM M1P. Substrate inhibition was evident at high maltohexaose concentrations. The smooth line represents the fit to the data using the Michaelis-Menten equation modified to allow for substrate inhibition. **F)** GlgE activity was determined as a function of M1P concentration using 1 mM maltohexaose. No substrate inhibition was observed with M1P. The smooth line represents the fit to the data using the Michaelis-Menten equation. All data points represent means of triplicate measurements and standard errors.

respectively (Fig 4A and 4B). The enzyme preferentially extended linear maltooligosaccharides with a degree of polymerisation (DP) of 5–7 (Fig 4C). The enzyme exhibited disproportionation activity with maltohexaose, yielding both longer and shorter oligosaccharides by two glucose residues (Fig 4D) as reported for GlgE enzymes from other bacteria [26, 57]. This side reaction is likely responsible for the substrate inhibition observed with maltohexaose in the polymerase reaction with M1P. Thus, the kinetic constants associated with maltohexaose extension by 1 mM M1P were k_{cat}^{app} 23 ± 1 s⁻¹, K_m^{app} 3.2 ± 0.4 mM and K_i^{app} 171 ± 26 mM

(Fig 4E). With 1 mM maltohexaose, the kinetic constants for M1P were k_{cat}^{app} 4.3 ± 0.3 s^{-1} and K_m^{app} 0.4 ± 0.1 mM (Fig 4F). These values are in the same range as those reported for GlgE enzymes from actinomycetes [57].

PAO1 TreY and TreZ convert α-glucan into trehalose

TreY is predicted to catalyse the conversion of the reducing-end α-1,4 linkage of α-glucan into an α-1,α-1-linkage, forming maltooligosyltrehalose. Trehalose is in turn predicted to be liberated from maltooligosyltrehalose by the hydrolase TreZ. Deletion of *treY* and *treZ* would be expected to block the production of trehalose leading to an accumulation of GlgA-derived α-glucan. This was indeed observed (Table 2 and S1 Fig). Deletion of *treZ* alone would be expected to lead to the accumulation of maltooligosyltrehalose. The appearance of a broad NMR signal at 5.2 ppm was consistent with the accumulation of the terminal α-1,1- linkage of this metabolite (S1 Fig). These data support the prediction that TreY and TreZ together generate trehalose from α-glucan. Unexpectedly, NMR signals corresponding to M1P were present in the PAO1 Δ*treY* and Δ*treZ* metabolomes, suggesting that a second, trehalose-independent route exists to form M1P.

MalQ disproportionates maltooligosaccharides and is capable of synthesising maltose

One possible trehalose-independent route to M1P in the Δ*treY/treZ* strain is *via* maltose derived from an activity other than TreS. The most likely candidate in PAO1 is the predicted α-glucanotransferase *malQ*, which is expected to transfer a portion of a maltooligosaccharide with a DP of ≥ 2 to an acceptor with a DP of ≥ 1. In other words, it would be capable of transferring a glucose group from the non-reducing end of a maltooligosaccharide donor to a glucose molecule acceptor to yield maltose. In addition, maltose can also be produced when maltotriose is the donor. The recombinant enzyme exhibited disproportionation activity when presented with maltohexaose. The products approached an entropy-driven distribution of products with degrees of polymerisation from DP ≤ 4 to DP ≥ 22 with the shortest products accumulating to the highest levels, according to MALDI mass spectrometry (Fig 5A). The matrix signals obscured products with a DP of ≤ 3, including maltose with its DP of 2. We therefore incubated MalQ with maltose to establish whether it was capable of interconverting maltose with other maltooligosaccharides. Indeed, it approached an entropy-driven distribution up to a DP of ≥ 10 associated with a proportionately lower average DP, as expected (Fig 5B). This illustrates that the shorter the average substrate is, the more abundant the shorter products are, for thermodynamic reasons [58]. Thus, glucose will enhance the level of maltose at equilibrium. To directly test the hypothesis that α-glucan can be converted to M1P using MalQ and TreS/Pep2, the enzymes were incubated with maltohexaose and ATP and the products were analysed using ^{1}H-NMR spectroscopy. M1P was indeed detected after 1 hour (Fig 5C). In addition, carrying out the reaction in the presence of coupling enzymes to monitor the production of ADP showed the reaction was several orders of magnitude quicker than the background rate of a control in the absence of MalQ. This result shows that MalQ could indeed bypass TreY/TreZ/TreS *in vivo*.

Deletion of the *malQ* gene in PAO1 would therefore be expected to increase the level of GlgA-derived α-glucan leading to increased flux through the TreY/TreZ route to trehalose, and a potentially lower net flux to M1P. The metabolome of this mutant was entirely consistent with these predictions (Table 2). Thus, MalQ directly contributes to the flux from GlgA-derived α-glucan to GlgE-derived α-glucan, which would be enhanced when glucose is also
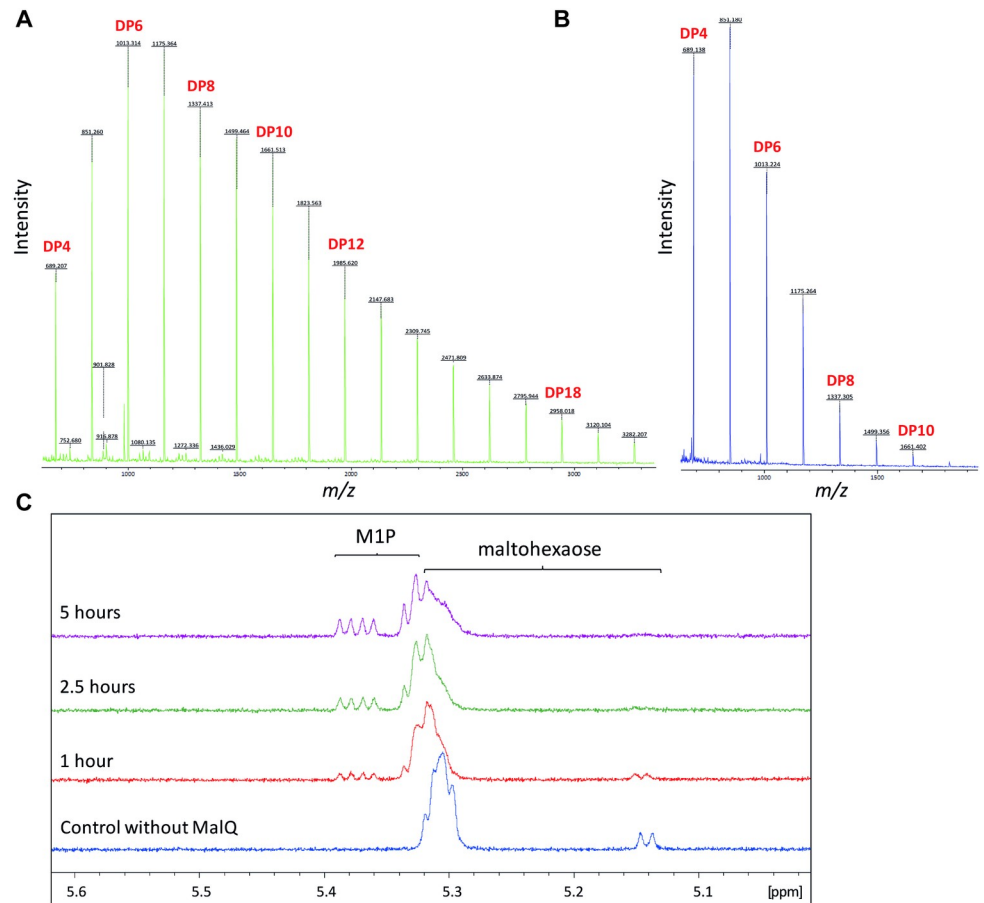
Fig 5. A) PAO1 MalQ is capable of disproportionating maltohexaose. MalQ was incubated with maltohexaose and the resulting reaction mixture was analysed using MALDI mass spectrometry. The DP of the maltooligosaccharide products formed is indicated. **B) PAO1 MalQ is capable of disproportionating maltose.** MalQ was incubated with maltose and the resulting reaction mixture was analysed using MALDI mass spectrometry. The DP of the maltooligosaccharide products formed is indicated. **C) Maltohexaose and ATP can be converted to M1P by PAO1 MalQ and TreS/Pep2.** MalQ and TreS/Pep2 were incubated with maltohexaose and ATP and the resulting reaction mixture was analysed using ¹H-NMR spectroscopy. Diagnostic resonances for M1P appeared concomitantly with the disappearance of those associated with maltohexaose (and other maltooligosaccharide intermediates).

present. Flux through this route would be enhanced when TreY and/or TreZ are blocked leading to an increase in the production of the MalQ α-glucan substrate derived from GlgA.

GlgB and GlgX introduce and hydrolyse α-1,6-linked branches in α-glucan particles, respectively

The branching enzyme GlgB is predicted to introduce branches into α-glucan by transferring a portion of a maltooligosaccharide to the 6-OH position of the same or a different α-glucan. Deletion of *glgB* should result in the absence of branched α-glucan and an accumulation of longer linear α-glucan chains and upstream metabolites. Indeed, PAO1 Δ*glgB* showed an increased level of trehalose, maltose/glucose, M1P (Table 2) and, (presumably linear) α-glucan (S1 Fig). To assess the length of linear α-glucan chains in PAO1 strains, we exposed colonies to iodine vapour [59]. Short linear chains do not stain, and branched polymers give a pale red/brown colour with iodine. PAO1 gave slight brown staining when exposed to iodine consistent with the production of branched α-glucan. By contrast, the *glgA* mutant gave essentially no
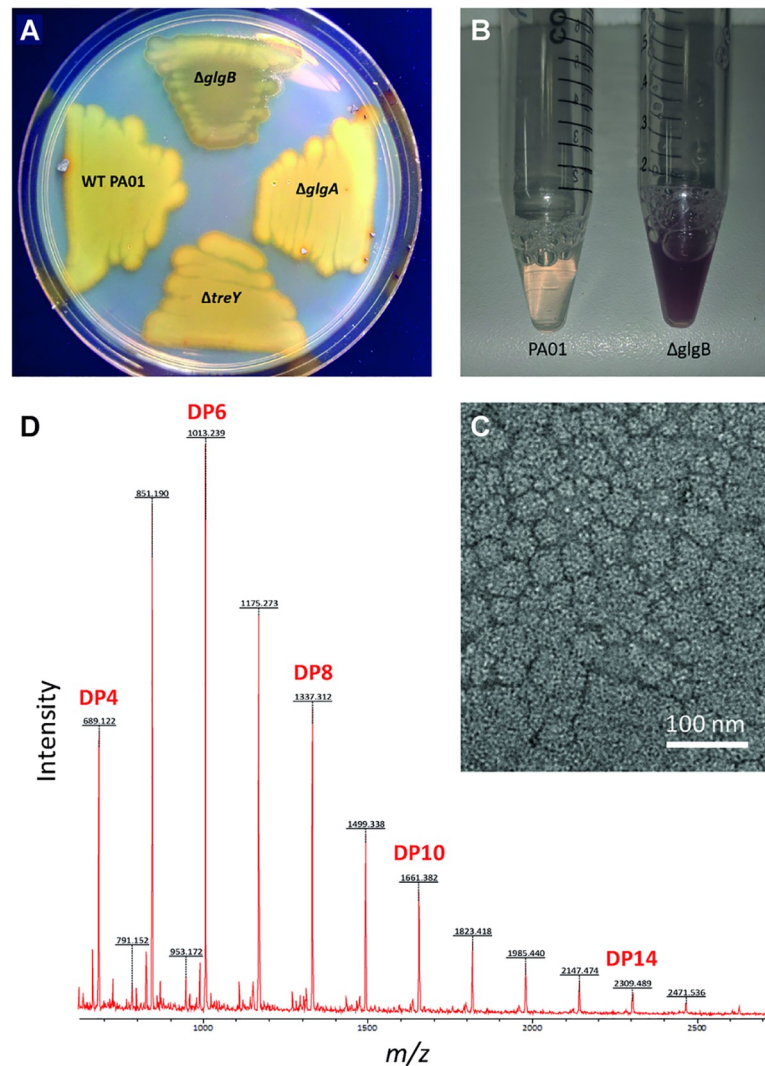
Fig 6. A) PAO1 strains exposed to iodine vapour. Δ*glgB* stains darker than the other tested strains due to the presence of insoluble linear α-glucan. **B) Lugol's solution** stains the Δ*glgB* sample dark purple **C) PAO1 GlgB and GlgE generate particles from maltohexaose and M1P.** GlgB and GlgE were incubated with maltohexaose and M1P and the resulting reaction mixture was analysed using transmission electron microscopy. Particles with diameters of tens of nm are evident. **D) Linear chain lengths of synthetic α-glucan.** The α-glucan particles generated by PAO1 GlgB and GlgE were exhaustively unbranched using isoamylase and analysed by MALDI mass spectrometry. The average DP of the chains was 7.6 ± 2.5 with a mode of 6.

https://doi.org/10.1371/journal.pgen.1009524.g006

staining consistent with a lack of α-glucan. Importantly, the Δ*glgB* strain stained a much darker colour than the wild-type strain, consistent with the presence of significant amounts of long linear α-glucan (Fig 6A). Similarly, the addition of Lugol's solution to the metabolite extract from the Δ*glgB* strain gave a dark purple colour associated with linear α-glucans with a DP of between 33 to 38 that are barely soluble (Fig 6B) [59]. Not only does this confirm the branching activity of GlgB, but also the production of α-glucan *in vivo*.

Recombinant PAO1 GlgB activity was investigated *in vitro* by incubating it with recombinant PAO1 GlgE, maltohexaose and M1P. Transmission electron microscopy of the resulting product mixture showed the presence of particles with diameters ranging from 20 to over 100 nm, with most around 40 nm (Fig 6C). These sizes are similar to those observed for particles

of α-glucan isolated from other bacteria or generated *in vitro* with GlgE and GlgB enzymes from other bacteria [60]. When the particles were hydrolysed using an isoamylase that cleaves all of the α-1,6 linkages, MALDI-MS revealed that the polymer was composed of linear chains with a mean DP of 7.6 ± 2.5 with a mode of 6 (Fig 6D). The chain length of α-glucan is largely dictated by the branching enzyme GlgB in such systems [60]. Importantly, these experiments show that the combination of GlgE and GlgB from PAO1 is capable of generating branched α-glucan particles.

The glycogen debranching enzyme GlgX is predicted to hydrolyse the α-1,6 links in branched α-glucan. Blocking this enzyme would severely restrict the recycling of branched α-glucan because the other enzymes that degrade the polymer can only operate on the α-1,4 link-ages of external chains. For example, although GlgP can in principle operate on all of the non-reducing ends of the arboreal α-glucan polymer, it can only do so until it gets to within a few glucose residues of the point where each external branch is attached to the rest of the polymer via an α-1,6 linkage. TreY and TreZ are even more restricted because they operate on reducing ends, of which an α-glucan polymer has only one. Furthermore, the reducing end can be steri-cally hindered by the rest of a mature polymer particle. Given the thermodynamics of the α-glucan pathways, a PAO1 Δ*glgX* mutant would be expected to accumulate branched α-glucan (i.e. a metabolic sink) at the expense of upstream metabolites. As predicted, the Δ*glgX* mutant showed a significant reduction in the levels of trehalose and M1P (Table 2). Unexpectedly, we saw no obvious signal for α-glucan in the Δ*glgX* mutant.

To examine the activity of recombinant PAO1 GlgX, it was incubated with rabbit liver gly-cogen composed of linear chains with a DP of 10.8 ± 4.6 [60]. MALDI-MS showed that the enzyme preferentially liberated a maltooligosaccharide with a DP of 4 and significantly less material with a DP of 5 and above (Fig 7), supporting its role as a debranching enzyme with a short chain-length specificity.

Distinguishing between linear α-glucan pools

At this stage it was unclear whether the linear α-glucan pools produced by GlgA or GlgE are structurally/ spatially distinct or if they are interchangeable. To try to distinguish between these two possibilities, we produced a GlgE pathway deletion mutant (i.e. missing the entire cluster comprising *glgE*, *treS/pep2* and *glgB* - Δ*PA2151-53*). Based on iodine staining (S2 Fig), this strain accumulated no more α-glucan than wild-type PAO1 (S2A and S2C Fig). To test whether MalQ modified the GlgA-derived α-glucan, the *malQ* gene was deleted in the GlgE pathway mutant strain background. However, no significant change in iodine staining was apparent in the resulting strain (S2E Fig). To test whether the GlgA-derived α-glucan pool was rapidly converted to trehalose, *treY* was deleted in the GlgE pathway mutant background (PAO1 Δ*4*). The significant blue staining of this strain with iodine (S2D Fig) showed that it accumulated long insoluble α-glucan chains with a DP of over 40 [59], longer than those detected in the *glgB* mutant. Thus, GlgA is capable of generating long linear α-glucan chains *in vivo* (with DPs that might be modified by MalQ). However, such GlgA-derived α-glucan does not accumulate in the cell unless its conversion to trehalose by TreY and TreZ is blocked. Overexpression of *glgB in trans* abolished the blue staining of the PAO1 Δ*4* mutant when exposed to iodine (S2F Fig), indicating that GlgA-derived α-glucan could be branched, and thus solubilised by GlgB, similarly to wild-type α-glucan.

Disruption of trehalose biosynthesis results in osmotic sensitivity in PAO1

Bacterial water stress manifests as at least two distinct phenomena: osmotic and desiccation stress [17]. Desiccation stress is distinct from osmotic stress in that it is independent of solute
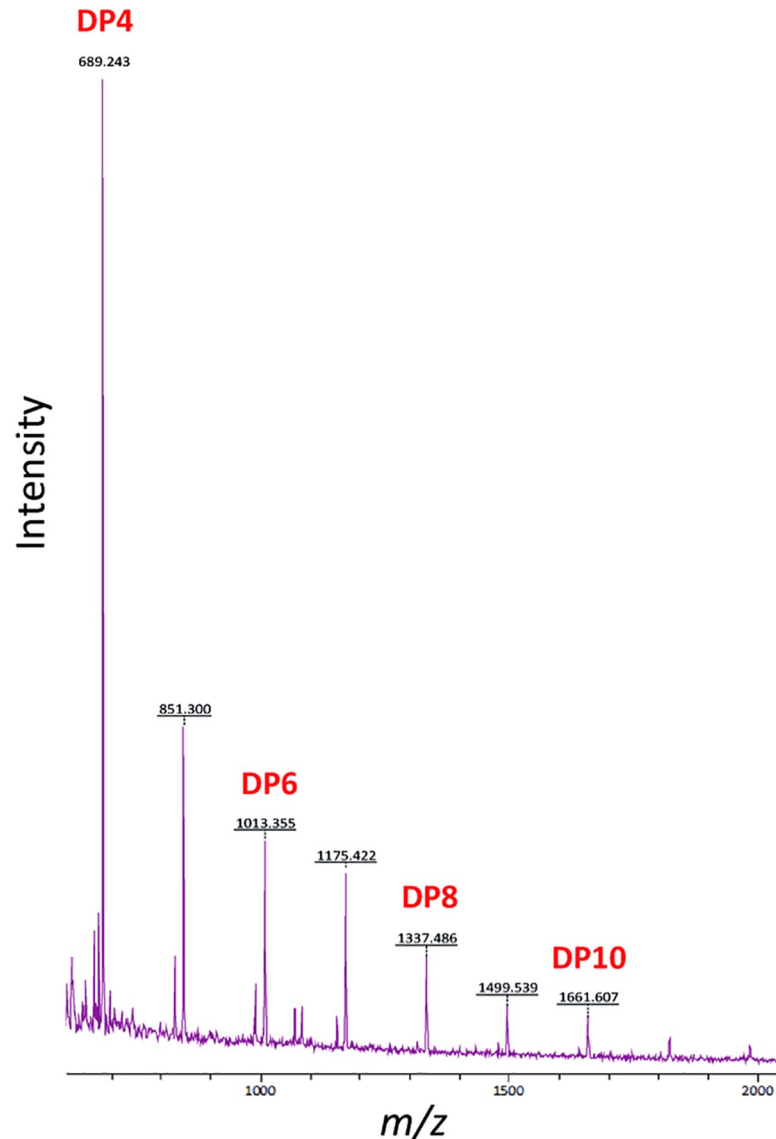
Fig 7. PAO1 GlgX is a debranching enzyme with a short chain length specificity. GlgX was incubated with rabbit liver glycogen that is composed of linear chains with an average DP of 10.8 ± 4.6. The resulting reaction mixture was analysed using MALDI mass spectrometry. The DP of the liberated linear maltooligosaccharide products is shown, with maltotetraose being the major product detected.

concentration: bacteria are exposed to air and water is lost to the atmosphere and cannot be recovered [61]. There is substantial overlap in the bacterial responses to these two stressors, although efforts have been made to distinguish individual responses from each other [62]. Trehalose has previously been associated with both osmotic and desiccation stress tolerance in *Pseudomonas* spp. [49, 50]. However, the newly revealed connection between trehalose and α-glucan metabolism begs the question as to whether α-glucan plays a direct role in mediating these phenotypes.

To investigate the association of trehalose and/or α-glucan with osmotolerance in PAO1, we first examined the effects of elevated salt on trehalose levels. PAO1 grown in M9 medium containing 0.85 M NaCl accumulated trehalose to 3.66 ± 1.11% of the cellular dry weight,

compared with 0.08 ± 0.02% for cells grown without added salt (S3 Fig and Table 2). Next, the growth of selected *glg* mutants were compared in the presence of elevated concentrations of salt (Fig 8). PAO1 grown in M9 minimal medium containing 0.85 M NaCl exhibited a severely delayed lag-phase but higher maximal density compared to growth without added NaCl (Fig 8A). PAO1 Δ*glgA* (trehalose⁻/α-glucan⁻) showed an even longer lag phase in the presence of salt than wild-type PAO1, consistent with trehalose and/or α-glucan conferring osmotolerance (Fig 8B). The Δ*treS*/*pep2* (trehalose⁺⁺, GlgE α-glucan⁻), Δ*glgE* (GlgE α-glucan⁻, Fig 8A), Δ*glgP* (GlgA α-glucan recycling, Fig 8C), and Δ*malQ* (trehalose⁺, Fig 8B) strains grew more similarly to the wild-type strain, implying trehalose rather than GlgE-derived α-glucan offered protection. Similarly, PAO1 Δ*treY* and Δ*treZ* (trehalose⁻, Fig 8B) showed significantly attenuated growth in elevated salt. Since the accumulated α-glucan in several of these strains would be expected to derive more from GlgA than GlgE, this result implies that the GlgA-derived α-glucan does not contribute to osmotolerance. The significant attenuation of the Δ*glgX* (trehalose⁻, Fig 8B) mutants again supports the role of trehalose in osmo-protection. Interestingly, the PAO1 Δ*glgB* mutant (trehalose⁺, Fig 8A) was also strongly attenuated in high-salt growth, despite this strain accumulating more trehalose than the wild-type strain (Table 2). This suggests that linear, insoluble α-glucan not only does not contribute to osmotolerance but may actually impede an effective osmostress response, perhaps due to reduced potential for metabolism to trehalose.

Loss of GlgE-derived α-glucan, but not trehalose, results in PAO1 desiccation sensitivity

Next, we assessed the ability of PAO1 mutants to survive exposure to prolonged periods of low relative humidity (RH). Colony forming units (CFU) recovered after exposure of bacterial samples to 100% and 75% RH were counted, with the resulting data analysed using linear mixed modelling and represented as predicted means of $\log_{10}(\text{CFU/ml})$, given the statistical model and the relevant model parameters. The sensitivity of a strain to lower humidity was calculated as the difference between its mean $\log_{10}(\text{CFU/ml})$ at 100% and at 75% RH. A greater response to lower RH of a mutant compared to the wild-type translates to a more desiccation-sensitive strain. Incubation of all PAO1 strains at 100% RH resulted in the recovery of means of 7.5–7.9 $\log_{10}(\text{CFU/ml})$. Incubation at 75% RH led to an approximately 10-fold reduction in the recovery of wild-type PAO1 to a mean of $\log_{10}(\text{CFU/ml}) = 6.5$ (Fig 9A), translating to a desiccation response of ~1.1 $\log_{10}(\text{CFU/ml})$.

It has previously been reported that trehalose contributes to desiccation tolerance in *P. aeruginosa* [22]. A Δ*glgA* mutant lacking all trehalose (and α-glucan) would therefore be expected to be more sensitive to desiccation than the wild-type strain. Incubation of PAO1 Δ*glgA* at 75% RH resulted in enhanced cell death with a reduction in cell recovery to 4.8 $\log_{10}(\text{CFU/ml})$ and a desiccation response of ~2.6 $\log_{10}(\text{CFU/ml})$. Surprisingly, the trehalose-producing, GlgE-derived α-glucan-null mutant PAO1 Δ*treS*/*pep2* showed a similar sensitivity to the Δ*glgA* mutant, with a desiccation response of ~3.1 $\log_{10}(\text{CFU/ml})$ (Fig 9A). This was despite this strain having a trehalose level nearly 7-fold higher than the wild-type strain (Table 2). This suggested that GlgE-derived α-glucan protects against desiccation stress. Interestingly, the PAO1 Δ*glgB* mutant also showed significantly ($p < 0.05$) enhanced desiccation tolerance, with a desiccation response of ~0.3 $\log_{10}(\text{CFU/ml})$, implying the GlgE-derived α-glucan did not need to be branched to afford protection (Fig 9A).

Overexpression of the *otsA* and *otsB* trehalose biosynthetic genes from *M. koreensis* 3J1 has previously been shown to increase trehalose production and confer increased desiccation resistance in *P. putida* [22, 63]. These genes were introduced into a strain lacking both α-glucan
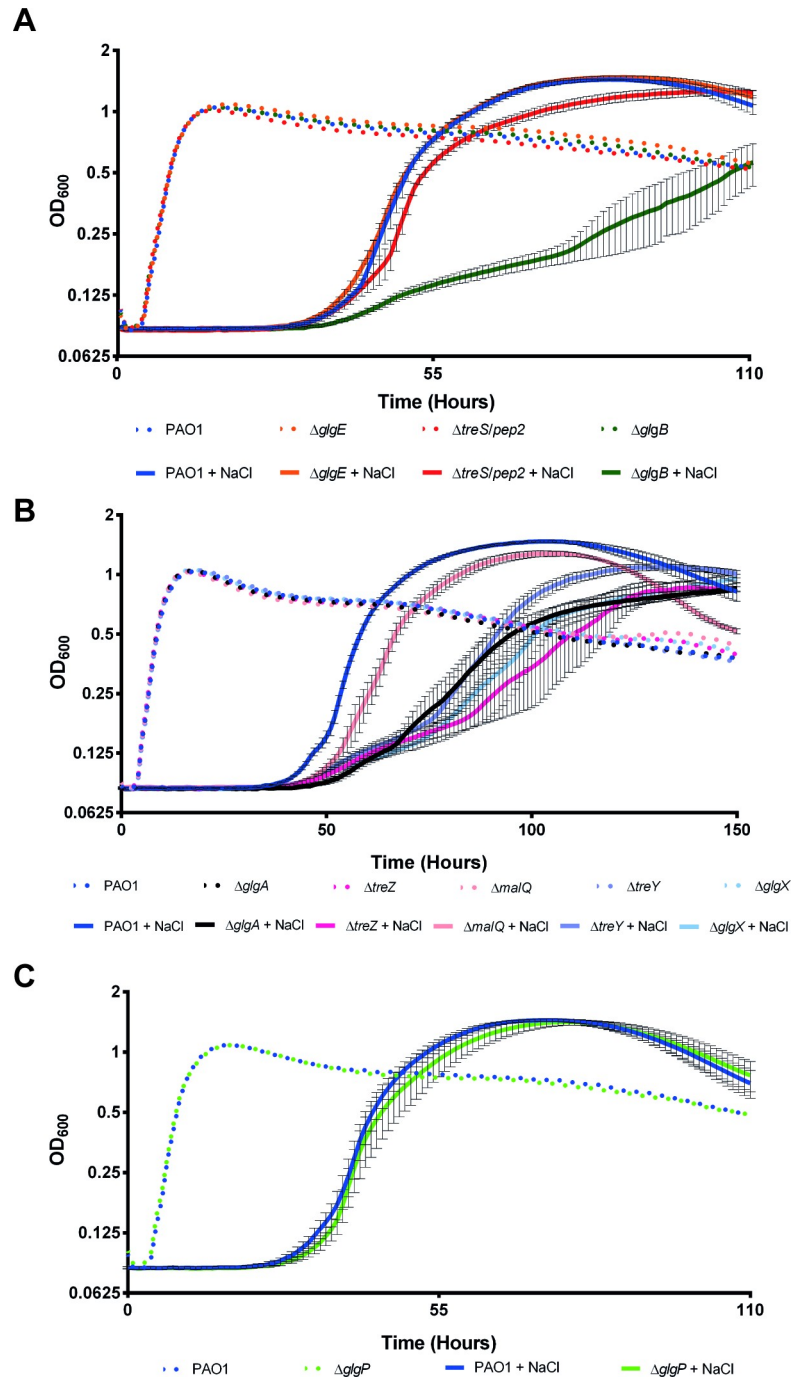
Fig 8. Growth curves of PAO1 mutant strains subject to osmotic stress conditions. OD_{600} is plotted against time for strains grown in the presence (+ NaCl, solid lines) and absence (dotted lines) of 0.85 M NaCl. Results are grouped according to the operon in which each set of genes is located: **A)** Wild-type (WT) PAO1, ΔglgE, ΔtreS/pep2 & ΔglgB. **B)** WT PAO1, ΔglgA, ΔtreZ, ΔmalQ, ΔtreY & ΔglgX **C)** WT PAO1 & ΔglgP. No growth defect relative to WT PAO1 was observed for any strain grown without NaCl. For strains grown in the presence of 0.85M NaCl, growth defects were seen for ΔglgB, ΔglgA, ΔtreZ, ΔtreY and ΔglgX. Data are shown +/- standard error of 3 technical replicates. At least two independent biological replicates were conducted per strain and a representative curve is shown in each case.

https://doi.org/10.1371/journal.pgen.1009524.g008
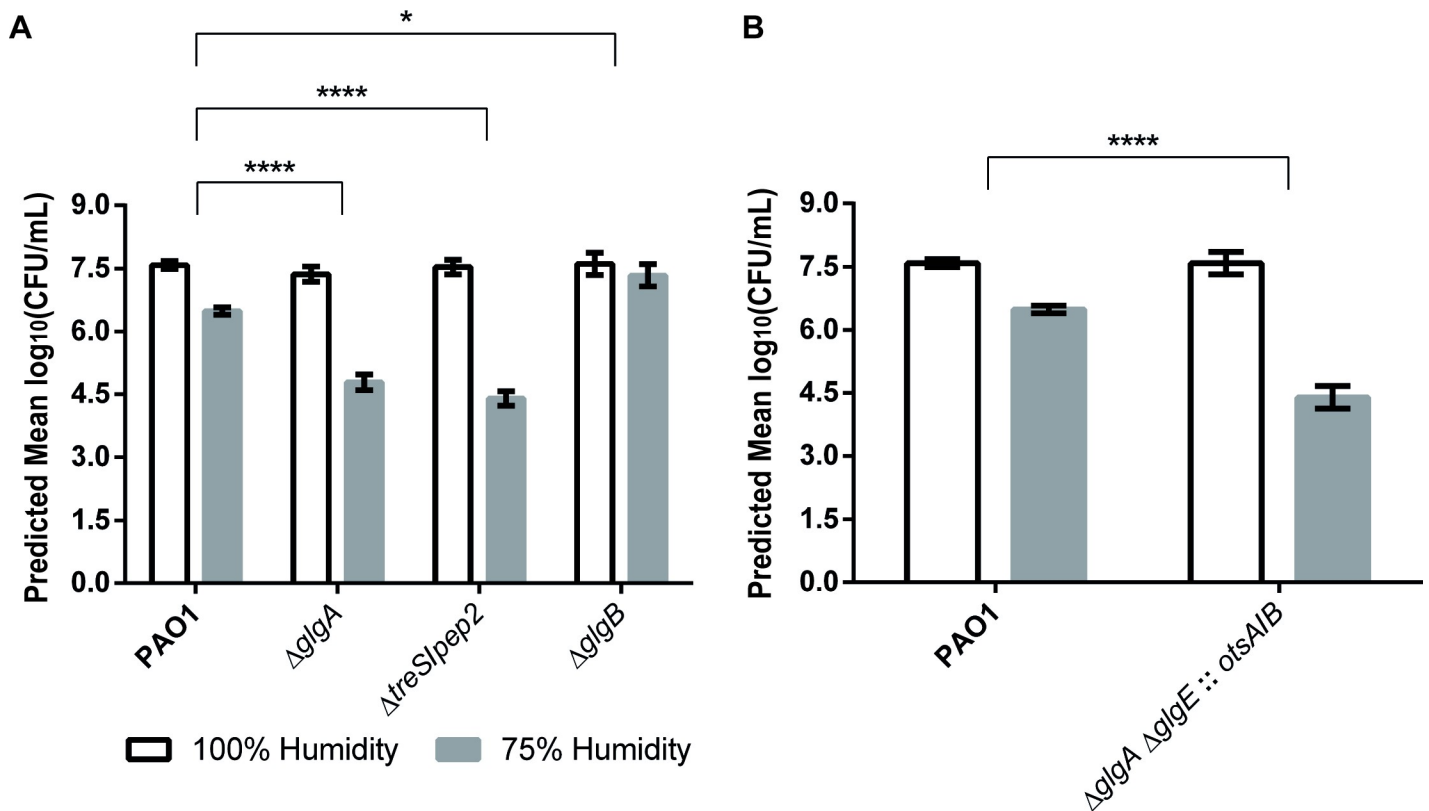
Fig 9. Survival of PAO1 mutant strains subject to desiccation stress conditions. Graphs show predicted mean log(CFU/ml) for strains grown in 100% (white bars) or 75% (grey bars) relative humidity. The response to desiccation is the difference log(CFU/ml) at 100% and 75% RH. P-values for differences between strains' responses were calculated by linear mixed modelling to account for the multiple levels of random variation in biological and technical replicates and are shown with asterisks (*: 0.05>p>0.01, ****: p<0.0001). Responses were tested in at least two independent biological replicates on different dates. **A)** Strains lacking GlgE-derived α-glucan (Δ*glgA*, Δ*treS/pep2*) are desiccation sensitive. Glucan branching (by GlgB) is not required for desiccation tolerance. **B)** Recovery of trehalose synthesis by *otsA/B* expression cannot recover desiccation tolerance in a Δ*glgA/E* (α-glucan minus) mutant.

https://doi.org/10.1371/journal.pgen.1009524.g009

polymerases (GlgA and GlgE) so that it was able to produce trehalose and, given the presence of TreS/Pep2, also maltose and M1P. This strain showed desiccation sensitivity comparable to the strain lacking TreS/Pep2, with a desiccation response of 3.2 $\log_{10}$(CFU/mL) ($p \leq 0.001$) (Fig 9B). This was despite the trehalose level ($0.07 \pm 0.02\%$, Table 2) being similar to that of wild-type PAO1. A significant ~2-fold increase in the M1P level to $0.66 \pm 0.11\%$ ($p \leq 0.05$) of cellular dry weight compared with the wild-type strain suggests that M1P does not contribute to desiccation stress tolerance in PAO1. Together, these results indicate that GlgE-derived α-glucan is a key mediator of *P. aeruginosa* desiccation tolerance, whether branched or not, and that trehalose does not directly offer protection.

Trehalose correlates with osmotolerance, while α-glucan correlates with desiccation tolerance

Our data show that the nearly 7-fold higher trehalose level in PAO1 Δ*treS/pep2* did not protect this strain against desiccation stress. This unexpected observation led us to explore the impact of increasing the level of trehalose in other strains on osmotolerance and desiccation tolerance. Consequently, *M. koreensis otsA* and *otsB* were constitutively expressed in PAO1 wild-type, Δ*glgA* and Δ*treS/pep2* strains and their effect on bacterial behaviour and metabolism was examined.

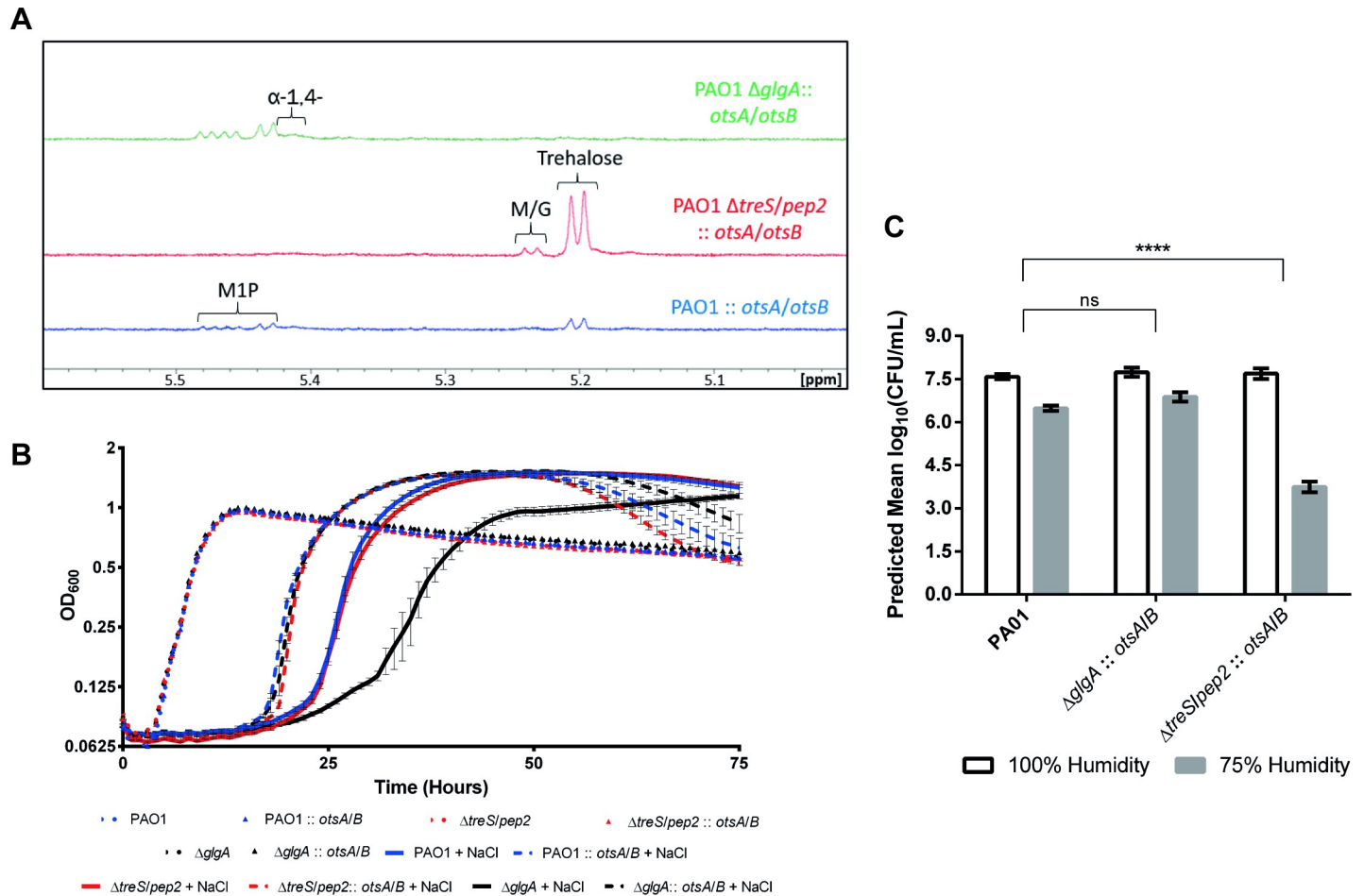**Fig 10. A) ^{1}H-NMR spectra for PAO1 strains expressing *otsA/B*.** Peaks corresponding to key metabolites are indicated. M/G–maltose/glucose, α-1,4-– α-glucan. **B) Growth curves of PAO1 strains expressing *otsA/B* subject to osmotic stress conditions.** OD_{600} is plotted against time for strains grown in the presence (+ NaCl, solid lines) and absence (dotted lines) of 0.85 M NaCl. Data are shown +/- standard error of 3 technical replicates. At least two independent biological replicates were conducted per strain and a representative curve is shown in each case. **C) Survival of PAO1 strains expressing *otsA/B* subjected to desiccation stress conditions.** Graphs show predicted mean log(CFU/ml) for strains grown in 100% (white bars) or 75% (grey bars) relative humidity. The response to desiccation is the difference log (CFU/ml) at 100% and 75% RH. P-values for differences between strains' responses were calculated by linear mixed modelling to account for the multiple levels of random variation in biological and technical replicates and are shown with asterisks (ns: $p > 0.05$ [not significant], ****: $p < 0.0001$). Responses were tested in at least two independent biological replicates on different dates.

https://doi.org/10.1371/journal.pgen.1009524.g010

Expression of *otsA/otsB* in PAO1 resulted in increased trehalose accumulation and a loss of M1P compared to wild-type PAO1 (Fig 10A). OtsA/OtsB and GlgA compete for the shared substrate UDP-glucose, so the GlgA-derived α-glucan level would be expected to decrease in this strain. In Δ*glgA*, OtsA/OtsB restored trehalose, M1P and α-glucan biosynthesis, which would be exclusively derived from GlgE. Expression of *otsA/otsB* in Δ*treS/pep2* resulted in a small increase in trehalose compared to the parental Δ*treS/pep2* mutant, while M1P and α-glucan could not be detected, as observed with Δ*treS/pep2* (Table 2). Expression of *otsA/otsB* did not affect the growth of any of these strains when no stress was applied. However, they were all strongly enhanced in their ability to tolerate osmotic stress compared to their respective parental strains lacking OtsA/OtsB (Fig 10B). This further supports the hypothesis that trehalose, rather than α-glucan, protects against osmotic stress in *Pseudomonas*.

The expression of *otsA/otsB* rescued the desiccation sensitivity exhibited by PAO1 Δ*glgA* (Fig 10C), resulting in a desiccation response of 0.9 $\log_{10}$(CFU/mL). This showed that either
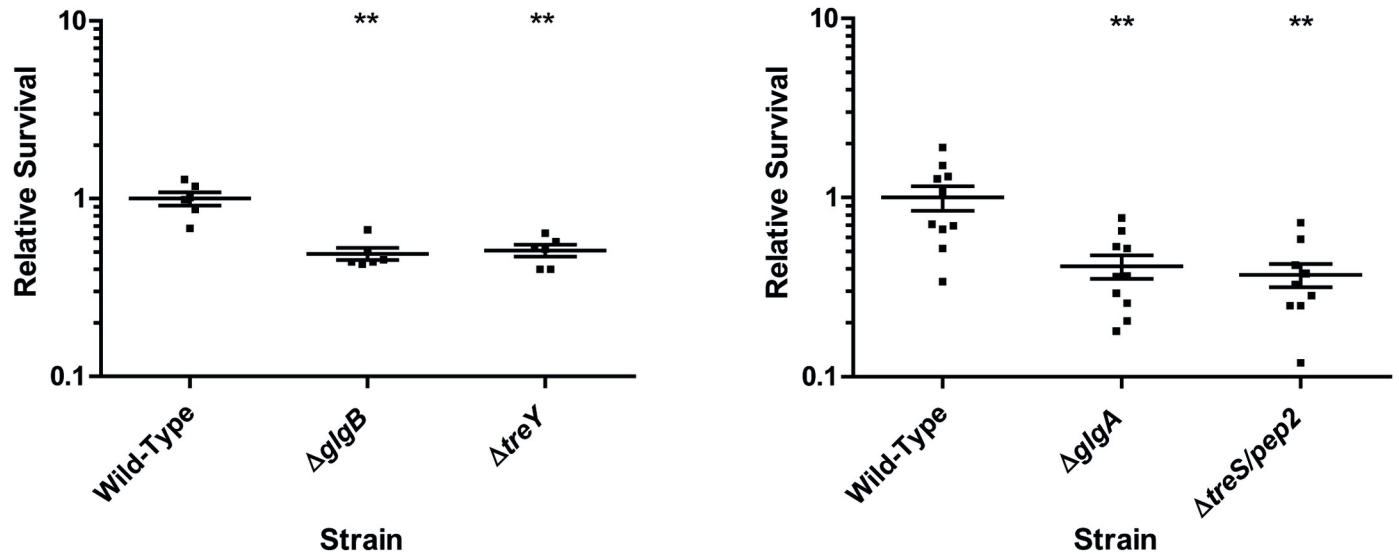
Fig 11. Survival of PAO1 mutant strains on a steel work surface. Scatter graphs showing recovered CFUs for PAO1 mutants after 24h incubation on a sterile brushed steel work surface, relative to WT PAO1. X-axis shows different *tre/glg* mutants, Y-axis shows recovered CFUs as a fraction of the mean WT value. Individual data points are shown, with mean values ± standard error indicated with bars. Significant differences from the WT are shown with asterisks (Mann-Whitney U test, **: p<0.01). Experiments were conducted at least twice independently for each mutant and representative assays versus WT PAO1 are shown in each case.

trehalose or GlgE-derived α-glucan confer tolerance to desiccation. In contrast, PAO1 Δ*treS/pep2::otsA/otsB* exhibited a desiccation response of approximately 4 $\log_{10}$(CFU/mL) ($p \leq 0.001$) translating to significant desiccation sensitivity compared to wild-type, despite accumulating trehalose to above wild-type levels (Fig 10A). Together our results strongly suggest that trehalose is not directly responsible for desiccation resistance in *Pseudomonas* spp. but rather exerts its desiccation tolerance effect indirectly through the biosynthesis of GlgE-derived α-glucan.

Trehalose and α-glucan contribute to *P. aeruginosa* survival on abiotic surfaces

Finally, we assessed the contribution of trehalose and α-glucan biosynthesis to *P. aeruginosa* survival in the wider environment. We sought to mimic the conditions these bacteria might encounter upon contaminating a kitchen countertop or other work surface. Therefore, 10 μl droplets of PAO1 strains were allowed to dry onto a sterile, brushed-steel worksurface, then recovered and quantified after 24h incubation at room temperature. Alongside wild-type PAO1 we examined the relative survival of Δ*glgA* (trehalose⁻, α-glucan⁻), Δ*glgB* (trehalose⁺, no branched glucan), Δ*treY* (trehalose⁻) and Δ*treS/pep2* (trehalose⁺, little/no α-glucan). These four strains were chosen to represent a range of different trehalose and α-glucan abundances and desiccation/osmostress tolerance states. Surprisingly, all four mutants were significantly compromised for surface survival compared with wild-type PAO1 (Fig 11), supporting roles for both trehalose and α-glucan biosynthesis in mediating *P. aeruginosa* survival on abiotic surfaces.

Discussion

The mechanisms that pathogenic bacteria use to tolerate external stresses are crucial to effective survival in the environment. In this study we characterise a central stress tolerance

pathway in a major opportunistic pathogen. Using a combination of reverse genetics and analytical biochemistry, we have deciphered the configuration of the *P. aeruginosa* trehalose and α-glucan biosynthetic pathways and differentiated between the contributions these ubiquitous molecules make to desiccation and osmotic stress tolerance (Fig 1B). To our knowledge, this is the first report characterising the mechanisms of trehalose and α-glucan biosynthesis and their physiological functions in an organism possessing both the GlgA and GlgE pathways.

GlgA catalyses the first committed step in this pathway, polymerising UDP-glucose into linear α-glucan. This GlgA-α-glucan is then rapidly degraded into trehalose by TreY and TreZ. TreY catalyses the conversion of the reducing-end α-1,4 bond of α-glucan into an α-1, α-1 glycosidic bond, forming maltooligosyltrehalose. This molecule is then hydrolysed by TreZ, liberating trehalose. Unexpectedly, M1P was detected in strains lacking functional TreY and TreZ despite the loss of trehalose biosynthesis, suggesting an alternative route exists to biosynthesise maltose. Consequently, we established that MalQ disproportionates α-glucan to produce maltose. This result reconciles the surprisingly low activity of the TreS domain of TreS/Pep2 because it offers an alternative and more direct route from GlgA-derived α-glucan to maltose. The clustering of the genes for all four enzymes in this part of the pathway would allow for coordinated transcriptional regulation. Since the production of maltose by MalQ would be enhanced by the presence of glucose, the configuration of the pathways in PAO1 with the kinetic bottleneck in TreS offers a potential advantage. When glucose is limiting, it would be expected that trehalose would be the main metabolite accumulated because neither MalQ nor TreS would be optimal in the generation of maltose. However, when glucose is abundant, much of the flux towards trehalose would be expected to be diverted to maltose via MalQ. The consequence is that GlgE-derived branched α-glucan could then accumulate.

Once M1P has been produced by TreS/Pep2 and polymerised into linear α-glucan by GlgE, GlgB introduces α-1,6 branch points to the linear chain to form branched α-glucan. Iterative rounds of extension and branching leads to the final product of the GlgE pathway. The genes for the three enzymes of this part of the pathway are clustered. Branched α-glucan is recycled by the phosphorylase GlgP, which degrades the non-reducing ends of α-glucan chains producing G1P, and the debranching enzyme GlgX. Due to steric constrains in the vicinity of branch points, phosphorylases such as GlgP are unable to degrade external chains with a DP of 4 or less [46]. However, we have shown that GlgX hydrolyses α-1,6 linked external branches with a preference for DP 4. It is therefore possible to generate branched polymer in the presence of GlgX, the gene for which is clustered with *glgA*, *treY*, *treZ* and *malQ*, provided the external chains have a DP > 4. Thus, PAO1 is capable of fully degrading branched α-glucan into glucose-1-phosphate when the orphaned gene *glgP* is expressed, allowing GlgP and GlgX to work together.

The GlgA and GlgE proteins in PAO1 and other *Pseudomonas* spp. enable two alternative mechanisms for linear α-glucan biosynthesis. We were unable to detect structural or functional differences between the α-glucan chains produced by either enzyme, with both molecules amenable to branching by GlgB and able to confer desiccation tolerance. On first inspection, the reasons for this apparent redundancy are unclear. However, despite producing α-glucan as an intermediate molecule, the cluster of genes including *glgA* is entirely geared towards the production of either trehalose or maltose *in vivo*. TreS/Pep2 deletion leads to an accumulation of intracellular trehalose, but this is not matched by a corresponding increase in GlgA-derived α-glucan due to rapid flux through TreY/TreZ that is assisted by a favourable equilibrium towards hydrolysis in the last step. This suggests that while GlgA and GlgE both produce α-glucan, the GlgA-produced molecule is rapidly metabolised before it forms mature particles. Thus, the vast majority of the large polymeric α-glucan accumulated by *P. aeruginosa* will be that produced by GlgE.

Trehalose and α-glucan biosyntheses in *Pseudomonas* spp. are clearly more closely integrated than previously suspected. Our analysis overturns earlier models for trehalose synthesis in *Pseudomonas* based on discrete sources of glycogen and maltose, with the source of the latter being previously unclear. Instead trehalose appears to be an intermediate that is both produced from and integral to the production of α-glucan via maltose (Fig 1B). Consequently, the intracellular levels of both molecules must be linked, with their relative abundance dependent both on the level of the other molecule and on the relative activity of the respective catabolic and anabolic enzymes. Controlling the balance between trehalose and α-glucan biosynthesis in *P. aeruginosa* is clearly central to an effective bacterial response to water stresses. In previous studies, trehalose has been extensively implicated in bacterial responses to both osmotic and desiccating conditions [49, 64–67]. Conversely, α-glucan has been very rarely associated with bacterial stress tolerance, with published roles in carbon and energy storage [68] and virulence [69]. In light of our findings, conventional models for trehalose-mediated stress tolerance in *Pseudomonas* need to be re-evaluated. Based on our revised understanding of the relationship between trehalose and α-glucan biosynthesis, we therefore revisited the roles of both molecules in mediating water stress phenotypes.

All tested PAO1 mutants that lacked the ability to synthesise trehalose were osmostress sensitive, confirming a role for trehalose in osmotic stress tolerance. This was irrespective of the α-glucan concentration, because the α-glucan over-accumulating Δ*treY* and Δ*treZ* mutants were both sensitive. While this suggests that α-glucan may not play a direct role in tolerance to osmostress, a PAO1 Δ*glgB* mutant lacking the α-glucan branching enzyme was also osmostress sensitive, despite its trehalose level exceeding those of wild-type PAO1 under unstressed conditions. It is possible that α-glucan may function as a substrate to ensure optimal trehalose production in response to osmostress. Alternatively, insoluble glucan functions as a major carbon sink. This may have wider metabolic and physical consequences for the cell, including osmostress sensitivity.

Although trehalose and α-glucan are biosynthetically linked, they have distinct roles in the protection of *Pseudomonas* spp. during water stress. By genetically decoupling cellular responses to distinct water stresses, we showed that trehalose contributes to osmotic stress protection in *Pseudomonas* spp., most likely due to its role as a compatible solute [18]. However, and contrary to previous reports, trehalose does not directly protect cells against desiccation. This function is instead attributed to the polysaccharide α-glucan. While the presence of trehalose correlates with protection against desiccation stress, this is only true when the cell retains the ability to process trehalose into α-glucan *via* the GlgE pathway. The loss of α-glucan biosynthesis resulted in desiccation sensitive strains, irrespective of the ability to synthesise trehalose. When the levels of intracellular GlgA- and GlgE-derived linear α-glucans are increased in the Δ*glgB* strain desiccation resistance was also increased. This suggests that α-glucan protects PAO1 against desiccation stress irrespective of branching. Intriguingly, despite the distinct stress response roles played by trehalose and α-glucan in *P. aeruginosa*, disruption of either biosynthetic pathway significantly compromised abiotic surface survival. This suggests that *Pseudomonas* survival in the environment relies on the integrated deployment of both stress tolerance molecules. This presents an attractive rationale for the close genetic integration of trehalose and α-glucan biosynthesis in *P. aeruginosa* and raises the possibility of targeting the GlgA/GlgE pathways to limit pathogen survival in clinical and other relevant settings.

Our findings have implications for models of trehalose metabolism and function in many bacterial species. GlgE pathway genes are present in around 14% of all sequenced bacterial genomes, including *Pseudomonas* spp. [48, 70, 71]. In the first instance, cell behaviours previously attributed to trehalose could in fact be mediated by α-glucan. For example, the

desiccation tolerance phenotype attributed to trehalose in *Bradyrhizobium japonicum* [23] may in fact be an α-glucan phenotype, as the *B. japonicum* genome contains a complete *glgE* operon. Similarly, trehalose has been implicated as a virulence factor in *P. syringae Pto* [49] and PA14 [50]. However, the mutations in both cases would also lead to abolition of α-glucan biosynthesis, raising the possibility that α-glucan plays a role in *Pseudomonas* virulence in a similar manner to *M. tuberculosis* [26].

There are still several outstanding questions concerning the role of trehalose and α-glucan in *P. aeruginosa*. At this stage the cellular localisation of α-glucan, and the mechanism by which it confers desiccation stress tolerance to PAO1 are unclear. *Pseudomonas fluorescens* has been shown to produce extracellular α-glucan [72] and mycobacterial α-glucan localises to both the cytosol and the extracellular capsule [36]. It is feasible that α-glucan acts as an exopolysaccharide (EPS) that PAO1functions as a hydrogel like the EPS molecule alginate, trapping water molecules and slowing their evaporation. Alternatively it may confer a structural role of some sort, preventing the loss of cell integrity as water levels decrease. These possibilities remain to be investigated.

The regulation of trehalose and α-glucan synthesis and deployment in *Pseudomonas* also largely remain to be determined. We show that *P. aeruginosa* trehalose production is massively stimulated by growth in a high salt environment. Trehalose biosynthesis is also stimulated by exposure to ethanol, via the alternative sigma factor AlgU and the signalling molecule (p) ppGpp [51]. Likewise, the GlgA and GlgE operons are upregulated in both PAO1 and *P. syringae Pto* under conditions associated with osmotic stress [67, 73], and during water stress in *P. putida* KT2440 [66]. However, the signalling pathways responsible for this, and the integration of their deployment with other stress response pathways and compatible solutes are currently undefined.

There is the potential for a futile cycle involving linear α-glucan being converted to trehalose and/or maltose and subsequently repolymerised to α-glucan at the expense of ATP. The main mechanism preventing this happening with branched polymer would be the requirement for GlgP activity to allow GlgX to debranch the polymer. However, linear α-glucan could also be cycled. The potential mechanisms to avoid this include a separation of GlgA and GlgE-derived linear α-glucan by time, space, or DP. It is feasible, for example, that short maltooligo-saccharides are preferentially degraded by TreY and TreZ and that longer ones are preferentially branched by GlgB (e.g. DP 14 [60]). This might be kinetically controlled by GlgA acting slowly and GlgE acting quickly and/or substrate specificity. In addition, it is possible that GlgE can extend branched polymers but GlgA cannot. Even with equal enzyme activities, GlgE would elongate at twice the rate, two glucose residues at a time. Note that we have shown that GlgE elongates both odd and even acceptor substrates, so its products would not have an exclusively even length. These issues require additional research.

Finally, the importance of trehalose and α-glucan during human infection by *P. aeruginosa* is unclear. Capsular α-glucan is known to be essential for the full virulence of *M. tuberculosis* in a murine model [37]. This involves the binding of α-glucan to phagocytic cells via complement receptor 3, the blocking of dendritic cell function, and interactions with the C-type lectin DC-SIGN. There is apparently a link between the evolution of *P. aeruginosa* mucoid phenotypes and a switch to trehalose utilisation as an osmoprotectant during chronic CF lung infections [52], although how this relates to infection success is unknown. PA14 *tre-* mutants were not attenuated in growth in a range of animal infection models [50]. However, these models are unlikely to reflect the significant osmolarity and desiccation stresses present in chronically infected CF lungs, or in the environmental reservoirs that contribute to the prevalence of community and hospital- acquired infections.

Materials and methods

Strains and growth media

Bacterial strains and plasmids used in this study are listed in S1 Table. *Pseudomonas aeruginosa* PAO1 and *Escherichia coli* DH5α strains were routinely cultured in lysogeny broth (LB, [74]) at 37˚C, solidified with 1.5% w/v agar where appropriate. Tetracycline was included in plates/media at 12.5 μg/ml for *E. coli* and 100 μg/ml for *P. aeruginosa*. Gentamycin was used at 25 μg/ml. For NMR spectroscopy and stress tolerance assays, PAO1 strains were grown in M9 medium (20 mM NH_4Cl, 12 mM Na_2HPO_4, 22 mM KH_2PO_4, 8.6 mM NaCl, 1 mM $MgSO_4$, 1 mM $CaCl_2$, supplemented with 0.4% glucose, 0.4% casamino acids and 50 μM $FeCl_3$) [74].

Molecular microbiology techniques

Cloning was carried out using standard molecular biology techniques [75]. Polymerase chain reaction (PCR) products and plasmid digestion derivatives were purified using NucleoSpin® Gel and PCR Clean-up kits (Macherey-Nagel). Plasmids were extracted from *E. coli* DH5α strains using the NucleoSpin® Plasmid DNA Purification kit (Macherey-Nagel). Cloning was performed using the appropriate restriction endonucleases and T4 DNA ligase (New England Biolabs). PCR reactions were conducted using Q5® High-Fidelity DNA polymerase (New England Biolabs). Primary denaturation was performed for 30 s at 98˚C. Following this, 30 cycles of denaturation (98˚C, 10 s), annealing (varying temperatures, 30 s) and extension (72˚C, 30 s) was performed, followed by a final extension at 72˚C for 120 s. The annealing temperature for a given reaction was calculated as $Tm_b - 2$˚C, where Tm_b represents the lowest Tm of the primer pair. The sequences and melting temperatures (Tm) of primers used in this study are listed in S2 Table.

Genetic manipulation of PAO1

Gene deletion vectors were constructed by amplifying the upstream and downstream regions flanking the desired gene from the PAO1 genome using primers 1–54 listed in S2 Table. Amplified up- and downstream flanking regions were then cloned into the multiple cloning site of the suicide vector pTS1 [76]. PAO1 cells were transformed with the appropriate deletion vectors following the method described in [77]. Single crossover integrations of each plasmid into the chromosome were selected on tetracycline plates and purified by re-streaking onto fresh plates. Single colonies were picked and grown overnight in 200 ml LB medium without selection. Colonies where double crossovers had occurred were then selected by plating onto LB agar with 10% w/v sucrose. Gene deletions were confirmed for tetracycline-sensitive, sucrose-resistant colonies by PCR using GoTaq® (Promega) and primers listed in S2 Table. The pME3087-derivative vector p*ΔPA2152* lacks the *sacB* counter-selection gene. In this case, we used tetracycline enrichment to select for double crossover candidates following the method described in [78] followed by PCR confirmation of successful gene deletions as described above.

To introduce *otsA/otsB* genes into the PAO1 *att::Tn7* site, the *otsA/otsB* locus was amplified from the *Microbacterium koreensis* 3J1 genome [63] using primers 55 and 56. The resulting PCR product was cloned into the multiple cloning site of pME6032 [79]. Primers 57 and 58 were then used to amplify *otsA/otsB* in addition to the *tac* promoter and terminator of pME6032. This product was then cloned into the pUC18-mini-*Tn7*T-Gm vector [80] and used to transform PAO1 via electroporation. To overexpress *glgB in trans*, the *glgB* open reading frame was amplified with primers 69 and 70 and cloned into plasmid pME6032 [79] between the *Eco*RI and *Xho*I sites. pME-*glgB* was then transferred into PAO1 strains by electroporation.

Enzymology

Unless otherwise stated, the genes coding for relevant enzymes were amplified from PAO1 genomic DNA by PCR with primers 58–68 & 71–72 and sub-cloned into a pET101 Directional TOPO vector (Invitrogen) allowing protein production with an N-terminal 6×His-tag. *E. coli* SoluBL21 cells (AMS Biotechnology Europe Ltd) bearing each resultant plasmid were grown in Lysogeny Broth to an OD_{600} of 0.6 (unless otherwise state) with agitation and recombinant gene expression was induced with 0.5 mM isopropyl β-D-thiogalactopyranoside (IPTG). Recombinant protein was purified using a 1 ml HisTrap FF column (GE Healthcare, Amersham, United Kingdom) with imidazole gradient elution. Purified proteins were buffer exchanged into 100 mM bis-tris propane, pH 7.0, containing 50 mM NaCl, unless otherwise stated.

The expression of recombinant PAO1 *glgA* was induced with IPTG and 0.4% dimethyl sulfoxide (DMSO). The culture was incubated for a further 5 hours at 37˚C with agitation. Purified GlgA was incubated with 10 mM NDP-glucose for 2 days at 20˚C. The product mixture was analysed using matrix-assisted laser desorption/ionisation-time of flight mass spectrometry by adding 1:1 (v/v) matrix (20 mg/ml 2,5-di-hydroxy-benzoic acid in 50:50 acetonitrile water) before spotting onto a Bruker MTP 384 Polished Steel TF target plate [60]. Spectra were acquired on Bruker Ultraflex or Autoflex Speed MALDI-TOF/TOF mass spectrometers (Coventry, United Kingdom), equipped with a pulsed nitrogen laser emitting at 337 nM or Smartbeam-II 2 kHz laser, respectively. Data were analysed using Bruker FlexAnalysis software. ^{1}H-NMR spectra were recorded as described below using samples that contained 10% (v/v) D_2O.

Recombinant PAO1 *glgP* was induced with IPTG and the culture was grown for a further 16 hours at 18˚C. Purified GlgP was buffer exchanged into 20 mM Hepes, pH 7.5. GlgP was incubated with 10 mM maltohexaose and 1 mM pyridoxal phosphate in 50 mM phosphate buffer, pH 7.0 at 20˚C for 18.5 hours. The reaction mixture was analysed using NMR spectroscopy.

Rather than cloning the PAO1 *treS/pep2* gene from genomic DNA, it was synthesised (Genscript Corporation, Piscataway, NJ, U.S.A.) with optimum codon usage for expression in *E. coli*, allowing the production of the enzyme with an N-terminal 6×His-tag with a TEV cleavage site. The synthetic gene was cloned into a pET-21a(+) (Novagen, Watford, United Kingdom) vector using *Nde*I and *BamH*I restriction sites. The expression of the recombinant enzyme in *E. coli* BL21(DE3) was induced with IPTG and 0.4% dimethyl sulfoxide (DMSO). The culture was incubated for a further 18 h at 18˚C with agitation. The protein was purified using a nickel-affinity column followed by an S200 16/60 gel filtration column (Pharmacia Biotech, Amersham, United Kingdom) eluted with 20 mM HEPES buffer, pH 7.5, containing 10% v/v glycerol and 200 mM NaCl. The maltokinase activity of TreS-Pep2 was monitored using a continuous enzyme-coupled spectrophotometric assay following the release of ADP. Chemicals were purchased from Sigma Aldrich. Unless otherwise stated, all enzyme assays were carried out at 21˚C in 50 mM bis-tris propane, pH 8.0, containing 5 mM MgCl₂, 0.3 mM NADH, 1 mM phosphoenolpyruvate, 1 U lactate dehydrogenase, 1 U pyruvate kinase and 0.2 mg/ml bovine serum albumin. The production of ADP was detected through the oxidation of NADH, whereby ADP is converted to ATP with phosphoenolpyruvate and pyruvate kinase acting in reverse, followed by pyruvate being reduced to lactate by lactate dehydrogenase. Saturation kinetics for ATP and maltose were measured in a 6 × 8 matrix in a Nunc 384 well plate using a BMG Clariostar plate reader. Six maltose concentrations were used from 0.125 to 4.0 mM and eight ATP concentrations from 8 μM to 1.0 mM. The effect of pH was measured using 50 mM buffers; bis-tris (pH 6.0) or bis-tris propane (pH 7.0, 8.0 and 9.0) with 1 mM ATP and 2 mM

maltose. The temperature-dependence of activity between 25 and 50˚C was determined using 1 mM ATP and 4 mM maltose using Perkin Elmer Lambda 25 or 35 spectrophotometers fitted with Peltier temperature controllers. Enzyme concentrations were such to allow reactions to progress linearly for 5 min (cuvette) or 100 s (plate reader) with total donor consumption being < 10%. Initial rates (v_0/[E]) were determined by monitoring the oxidation of NADH at 340 nm.

Kinetics curves were fitted to a random order bi-substrate ternary complex model (Eq 1) using global fitting in GraphPad Prism 8. The value for K_{mA} was obtained by repeating the fitting with all of the terms for A and B reversed, given the symmetry of the mechanism.

$$\frac{v_0}{[E]} = \frac{k_{cat}[A][B]}{K_{iA}K_{mB} + K_{mB}[A] + \frac{K_{iA}K_{mB}[B]}{K_{iB}} + [A][B]} \tag{1}$$

Recombinant PAO1 *glgE* was induced with IPTG and the culture was grown for a further 5 hours at 37˚C. GlgE activity was measured using a spectrophotometric stopped assay that detected the release of inorganic phosphate using Malachite green [26]. The effect of pH was measured using 20 mM buffers; bis-tris (pH 6.0) or bis-tris propane (pH 7.0, 8.0 and 9.0) with 0.25 mM M1P and 1 mM maltohexaose. The effect of temperature was measured with 1 mM each of M1P and maltohexaose. The default GlgE assays were carried out at 30˚C and a 1 mM fixed substrate concentration. Disproportion activity was detected using MALDI mass spectrometry.

Individual kinetic curves were fitted to either a Michaelis-Menten model (Eq 2) or one modified to include substrate inhibition (Eq 3) using GraphPad Prism 8.

$$\frac{v_0}{[E]} = \frac{k_{cat}[S]}{K_m + [S]} \tag{2}$$

$$\frac{v_0}{[E]} = \frac{k_{cat}[S]}{K_m + [S]\left(1 + \frac{[S]}{K_i}\right)} \tag{3}$$

Recombinant PAO1 *malQ* was induced with IPTG and the culture was grown for a further 16 hours at 18˚C. Purified MalQ was incubated with 1 mM substrate to test for disproportionation activity. Reaction mixtures were analysed using MALDI mass spectrometry. The production of maltose from maltohexaose was also tested using an assay coupled to the production of M1P and ADP by TreS/Pep2 as described above. Specifically, MalQ was incubated with TreS/Pep2, 1 mM ATP, 5 mM maltohexaose, 1 U lactate dehydrogenase, 1 U pyruvate kinase, 1 mM phosphoenol pyruvate, 0.3 mM NADH, 50 mM bis-tris propane, pH 7.0, and 5 mM MgCl$_2$. Similarly, MalQ was incubated with TreS/Pep2, 1 mM maltohexaose, 4 mM ATP and 0.2 mg/ml bovine serum albumin, and the reaction mixture was analysed using NMR spectroscopy to detect the production of M1P.

Recombinant PAO1 *glgB* was induced in auto-induction medium [81] and incubated for 5 hours at 37˚C. Purified GlgB was incubated with PAO1 GlgE, 1 mM maltohexaose, and 10 mM M1P for 2 days at 20˚C. The resulting α-glucan particles were analysed using transmission electron microscopy after staining with 2% aqueous uranyl acetate, pH 4.5 [60]. Samples were also buffer exchanged into sodium acetate buffer, pH 4.0, using 10 kDa cut-off filters that removed maltohexaose and M1P. The washed particles were digested with 2 U of isoamylase for 3 hours at 37˚C [60]. The resulting product mixtures were analysed using MALDI mass spectrometry.

Recombinant PAO1 *glgX* was induced with IPTG and the culture was grown for a further 16 hours at 18˚C. Purified GlgX was incubated with 10 mg/ml rabbit liver glycogen in 20 mM bis-tris propane, pH 7.0. The resultant product mixture was analysed using MALDI mass spectrometry. Control reactions without GlgX contained no detectable maltooligosaccharides.

Metabolite extraction

Overnight PAO1 cultures were grown in M9 medium at 37˚C with shaking, then diluted to an OD_{600} of 0.5 in PBS. Mixed cellulose ester filter discs (Merck Millipore) were placed on the surface of M9 agar plates and coated with the diluted cell suspensions. Plates were then incubated at 37˚C for 16 hours before cells were harvested from each disc and resuspended in 5 ml of ddH_2O in a 15 ml plastic tube by vigourous vortexing. To measure the effect of added NaCl, 250 mL flasks containing 50 mL M9 medium ± 0.85M NaCl were inoculated with overnight PAO1 cultures and grown at 37˚C with shaking for 96 hours, before pelleting and resuspension in ddH_2O as above. Water was then removed from each sample by drying under vacuum for 16 hours. Following this step, sample dry weight was determined. Dried cells were resuspended in ddH_2O and boiled at 95˚C for 20 minutes. Boiled cells were then centrifuged ($10,000 \times g$, 10 minutes) and the resulting supernatant was subject to additional boiling and centrifugation steps. The supernatant, now containing the total soluble metabolite content of the cell sample, was dried under vacuum for a further 16 hours. The resulting dried pellet was resuspended in 1200 μl deuterium oxide (D_2O) and analysed by NMR spectroscopy.

Nuclear magnetic resonance spectroscopy

Metabolite samples from cell extracts were subjected to ^{1}H-NMR spectroscopy using a Bruker AVANCE III 400 spectrometer. Samples were examined at room temperature using 400 MHz with water suppression. Metabolite chemical shifts were recorded as parts per million (ppm) compared to the standard: 0.5 mM trimethylsilyl propanoic acid (TMSP; 0.00 ppm). Spectra were analysed using Topspin 3.0 (Bruker) and the concentrations of trehalose and M1P were established through the manual integration of their resonances relative to TMSP. The resonances were assigned based on previously established spectra [82]. See relevant figures for representative spectra.

α-Glucan staining

The production of α-glucan in PAO1 colonies was visualised with iodine crystals (Sigma-Aldrich). A few crystals were placed in the lids of inverted plates upon which bacterial strains were streaked. Strains were placed in a fume hood and exposed to sublimating iodine vapour for 2 minutes and were immediately photographed. α-Glucan in metabolite extracts was visualised by adding 15% (v/v) Lugol's solution (Sigma-Aldrich).

Osmotic stress assays

The growth kinetics of each bacterial strain were measured using a temperature controlled 96-well microplate spectrometer (Biotek Instruments). Overnight PAO1 cultures were grown in M9 medium (20 mM NH_4Cl, 12 mM Na_2HPO_4, 22 mM KH_2PO_4, 8.6 mM NaCl, 1 mM $MgSO_4$, 1 mM $CaCl_2$, and 0.4% glucose, 0.4% casamino acids, 50 μM $FeCl_3$) at 37˚C with shaking, then diluted to OD_{600} of 0.01 in M9 medium. Five μl of each diluted sample was used to inoculate 150 μl of M9 medium. To examine osmotic stress conditions, growth media were supplemented with 0.85 M NaCl. Growth in 96-well plates at 37˚C was monitored by

measuring the OD_{600} every hour until stationary phase had been attained. Assays were conducted in triplicate and repeated at least twice independently, with a representative sample shown in each case.

Desiccation tolerance assays

Overnight PAO1 cultures were grown in M9 medium at 37°C with shaking, then diluted to an OD_{600} of 0.1 in PBS. Ten μl of each culture were spotted onto 15 mm grade 1 Whatman filter discs (GE Healthcare Life Sciences). After drying for 1 minute at room temperature, discs were placed onto M9 agar plates and incubated at 37°C for 4 hours to enable bacteria to recover and begin dividing. After incubation, the filter discs were subjected to controlled desiccation in tightly sealed bell chambers containing either water (100% RH) or a saturated solution of NaCl (75% RH [83]) for 2 hours. Bacteria were then recovered from filter discs in 3 ml of PBS and serially diluted onto LB agar plates. The number of colony-forming units (CFU) were determined for each strain. Assays were conducted in triplicate (technical replicates) and repeated at least twice independently on different dates (biological replicates).

Surface survival assays

Overnight PAO1 cultures were grown in LB medium at 37°C with shaking, washed once with PBS, then diluted to an OD_{600} of 1.0 in PBS. The number of colony-forming units (CFU) was determined for each strain by serial dilution onto LB agar plates. Ten μl of each culture were spotted onto a sterile, brushed steel work surface and allowed to dry. Spots were incubated for 24 h at room temperature and in ambient atmospheric conditions (Norwich, UK, August 2020). Bacteria were then recovered in 10 μl of PBS and serially diluted onto LB agar plates. The number of colony-forming units (CFU) was determined for each strain and normalised to the CFU of the initial inoculum. Assays were conducted with at least six replicates per sample and repeated twice independently.

Statistical analysis of desiccation data

Log_{10}(CFU) values from the desiccation assays were analysed by linear mixed modelling using restricted maximum likelihood (REML). Modelling by REML is a standard method of calculating means, standard errors, and confidence intervals for treatments of interest (here, the experimental conditions and bacterial strains) when the experiment has multiple sources of random variation (here, biological replicates and technical replicates). Predicted means for conditions and strains account for the effect of the experimental design. The random effect was Date of experiment and the fixed effects were Condition*Strain, where * is the crossing operator. Condition included the initial culture (T_0) and growth at 100% RH and 75% RH. The three technical replicate samples with the same Condition and Strain tested on the same Date provided the residual error term. The statistical significance of Condition, Strain and their interaction was determined by F-tests of Wald statistics. The response of a strain to lower humidity was calculated as the difference between its predicted mean log_{10}(CFU) at 100% RH and at 75% RH. The standard error of the difference (SED) between the responses of mutant and wild-type strains was calculated from the appropriate standard errors (SE) with the formula: SED = (SE [100%, Mutant]^2 + SE[75%, Mutant]^2 + SE[100%, wild-type]^2 + SE[75%, wild-type]^2)$^{0.5}$. The significance of the response difference was tested using the normal distribution with a variance of SED^2. Statistical significance between the desiccation responses of all PAO1 strains is summarised in **S3** Table.

Supporting information

S1 Fig. Illustrative ^{1}H-NMR spectra for PAO1 *glgA* and *glgE* operon mutants. Peaks corresponding to key metabolites: M/G–maltose/glucose, α-1,4-– α-glucan, α-1,1-–probable terminal linkage of maltooligosyltrehalose. Mutant strains are labelled as follows: **A)** Δ*glgE*, **B)** Δ*treS/pep2*, **C)** Δ*glgB*, **D)** Δ*glgA*, **E)** Δ*treZ*/Δ*treY*, **F)** Δ*malQ*, **G)** Δ*glgX*, **H)** Δ*glgP*, **I)** Δ*glgA* Δ*glgE*:: *otsA/otsB*.
(TIF)

S2 Fig. PAO1 strains exposed to iodine vapour. Strains producing insoluble linear α-glucan stain blue-purple. Mutant strains are labelled as follows: **A)** Wild-type PAO1, **B)** Δ*glgB*, **C)** Δ*PA2151-53*, **D)** Δ*treY* Δ*PA2151-53* (PAO1 *Δ4*), **E)** Δ*malQ* Δ*PA2151-53*, **F)** PAO1 *Δ4* pME-*glgB*.
(TIF)

S3 Fig. Illustrative ^{1}H-NMR spectra for wild-type PAO1 grown with and without 0.85M NaCl. The peak corresponding to trehalose is indicated.
(TIF)

S1 Table. Strains and plasmids used in this study.
(DOCX)

S2 Table. Primers used in this study.
(DOCX)

S3 Table. Statistical significance between the desiccation responses of PAO1 and mutant strains. Predicted means and standard errors of $\log_{10}$(CFU/ml) for desiccation assays in Figs 9 and 10, calculated by linear mixed modelling (see text for details). The response to desiccation is the difference between $\log_{10}$(CFU) at 100% and 75% RH. P-values were calculated by Z-tests using the normal distribution.
(DOCX)

Acknowledgments

We thank Sibyl Batey for assistance with data analysis.

Author Contributions

Conceptualization: Stuart D. Woodcock, Karl Syson, Stephen Bornemann, Jacob G. Malone.

Data curation: James K. M. Brown, Stephen Bornemann.

Formal analysis: Stuart D. Woodcock, Karl Syson, James K. M. Brown, Stephen Bornemann, Jacob G. Malone.

Funding acquisition: Stephen Bornemann, Jacob G. Malone.

Investigation: Stuart D. Woodcock, Karl Syson, Richard H. Little, Danny Ward, Despoina Sifouna, Jacob G. Malone.

Methodology: Stuart D. Woodcock, Karl Syson, Richard H. Little, Jacob G. Malone.

Project administration: Jacob G. Malone.

Resources: Stephen Bornemann, Jacob G. Malone.

Supervision: Richard H. Little, Stephen Bornemann, Jacob G. Malone.

Writing – original draft: Stuart D. Woodcock, Jacob G. Malone.

Writing – review & editing: Stuart D. Woodcock, Karl Syson, Richard H. Little, James K. M. Brown, Stephen Bornemann, Jacob G. Malone.

References

1. Liu W-P, Tian Y-Q, Hai Y-T, Zheng Z-N, Cao Q-L. Prevalence survey of nosocomial infections in the Inner Mongolia Autonomous Region of China [2012–2014]. Journal of Thoracic Disease. 2015; 7 (9):1650–7. https://doi.org/10.3978/j.issn.2072-1439.2015.09.41 PMID: 26543614

2. Centres for Disease Control and Prevention. *Antibiotic Resistance Threats in the United States*, *2013*. Atlanta: Centres for Disease Control and Prevention, 2013.

3. Kielhofner M, Atmar RL, Hamill RJ, Musher DM. Life-Threatening *Pseudomonas aeruginosa* Infections in Patients with Human Immunodeficiency Virus Infection. Clinical Infectious Diseases. 1992; 14 (2):403–11. https://doi.org/10.1093/clinids/14.2.403 PMID: 1554824

4. Chitkara YK, Feierabend TC. Endogenous and exogenous infection with *Pseudomonas aeruginosa* in a burns unit. International surgery. 1981; 66(3):237–40. Epub 1981/07/01. PMID: 6797982.

5. Shigemura K, Arakawa S, Sakai Y, Kinoshita S, Tanaka K, Fujisawa M. Complicated urinary tract infection caused by *Pseudomonas aeruginosa* in a single institution (1999–2003). International Journal of Urology. 2006; 13(5):538–42. https://doi.org/10.1111/j.1442-2042.2006.01359.x PMID: 16771722

6. Williams BJ, Dehnbostel J, Blackwell TS. *Pseudomonas aeruginosa*: host defence in lung diseases. Respirology (Carlton, Vic). 2010; 15(7):1037–56. Epub 2010/08/21. https://doi.org/10.1111/j.1440-1843.2010.01819.x PMID: 20723140.

7. Pressler T, Bohmova C, Conway S, Dumcius S, Hjelte L, Høiby N, et al. Chronic *Pseudomonas aeruginosa* infection definition: EuroCareCF Working Group report. Journal of Cystic Fibrosis. 2011; 10:S75–S8. https://doi.org/10.1016/S1569-1993(11)60011-8 PMID: 21658646

8. Henry RL, Mellis CM, Petrovic L. Mucoid *Pseudomonas aeruginosa* is a marker of poor survival in cystic fibrosis. Pediatric Pulmonology. 1992; 12(3):158–61. https://doi.org/10.1002/ppul.1950120306 PMID: 1641272

9. Conway SP, Lee TW. Prevention of chronic *Pseudomonas aeruginosa* infection in people with cystic fibrosis. Expert Review of Respiratory Medicine. 2009; 3(4):349–61. Epub 2010/05/19. https://doi.org/10.1586/ers.09.26 PMID: 20477327.

10. Beales N. Adaptation of microorganisms to cold temperatures, weak acid preservatives, low pH, and osmotic stress: A review. Comprehensive Reviews in Food Science and Food Safety. 2004; 3(1):1–20. https://doi.org/10.1111/j.1541-4337.2004.tb00057.x PMID: 33430556

11. Pérez V, Hengst M, Kurte L, Dorador C, Jeffrey WH, Wattiez R, et al. Bacterial Survival under Extreme UV Radiation: A Comparative Proteomics Study of Rhodobacter sp., Isolated from High Altitude Wetlands in Chile. Frontiers in microbiology. 2017; 8:1173–. https://doi.org/10.3389/fmicb.2017.01173 PMID: 28694800.

12. Bhagirath AY, Li Y, Somayajula D, Dadashi M, Badr S, Duan K. Cystic fibrosis lung environment and *Pseudomonas aeruginosa* infection. BMC Pulmonary Medicine. 2016; 16(1):174. https://doi.org/10.1186/s12890-016-0339-5 PMID: 27919253

13. Mann EE, Wozniak DJ. *Pseudomonas* biofilm matrix composition and niche biology. FEMS Microbiology Reviews. 2012; 36(4):893–916. Epub 2012/01/23. https://doi.org/10.1111/j.1574-6976.2011.00322.x PMID: 22212072.

14. Deng X, Li Z, Zhang W. Transcriptome sequencing of *Salmonella enterica* serovar Enteritidis under desiccation and starvation stress in peanut oil. Food Microbiology. 2012; 30(1):311–5. https://doi.org/10.1016/j.fm.2011.11.001 PMID: 22265317

15. Kintz E, Goldberg JB. Regulation of lipopolysaccharide O antigen expression in Pseudomonas aeruginosa. Future Microbiol. 2008; 3(2):191–203. Epub 2008/03/28. https://doi.org/10.2217/17460913.3.2.191 PMID: 18366339.

16. Battista JR, Park M-J, McLemore AE. Inactivation of two homologues of proteins presumed to be involved in the desiccation tolerance of plants sensitizes *Deinococcus radiodurans* R1 to desiccation. Cryobiology. 2001; 43(2):133–9. https://doi.org/10.1006/cryo.2001.2357 PMID: 11846468

17. Wood JM. Bacterial responses to osmotic challenges. The Journal of General Physiology. 2015; 145 (5):381–8. https://doi.org/10.1085/jgp.201411296 PMID: 25870209

18. Elbein AD, Pan YT, Pastuszak I, Carroll D. New insights on trehalose: a multifunctional molecule. Glycobiology. 2003; 13(4):17R–27R. https://doi.org/10.1093/glycob/cwg047 PMID: 12626396

19. Larsen PI, Sydnes LK, Landfald B, Strøm AR. Osmoregulation in *Escherichia coli* by accumulation of organic osmolytes: betaines, glutamic acid, and trehalose. Archives of microbiology. 1987; 147(1):1–7. https://doi.org/10.1007/BF00492896 PMID: 2883950

20. Reina-Bueno M, Argandoña M, Salvador M, Rodríguez-Moya J, Iglesias-Guerra F, Csonka LN, et al. Role of Trehalose in Salinity and Temperature Tolerance in the Model Halophilic Bacterium *Chromohalobacter salexigens*. PLoS ONE. 2012; 7(3):e33587. https://doi.org/10.1371/journal.pone.0033587 PMID: 22448254

21. Zhang Q, Yan T. Correlation of intracellular trehalose concentration with desiccation resistance of soil Escherichia coli populations. Appl Environ Microbiol. 2012; 78(20):7407–13. Epub 2012/08/14. https://doi.org/10.1128/AEM.01904-12 PMID: 22885754; PubMed Central PMCID: PMC3457116.

22. Vílchez JI, García-Fontana C, Román-Naranjo D, González-López J, Manzanera M. Plant Drought Tolerance Enhancement by Trehalose Production of Desiccation-Tolerant Microorganisms. Frontiers in Microbiology. 2016; 7:1577. https://doi.org/10.3389/fmicb.2016.01577 PMC5043138. PMID: 27746776

23. Sugawara M, Cytryn EJ, Sadowsky MJ. Functional role of Bradyrhizobium japonicum trehalose biosynthesis and metabolism genes during physiological stress and nodulation. Appl Environ Microbiol. 2010; 76(4):1071–81. Epub 2009/12/22. https://doi.org/10.1128/AEM.02483-09 PMID: 20023090; PubMed Central PMCID: PMC2820964.

24. Kuczynska-Wisnik D, Stojowska K, Matuszewska E, Leszczynska D, Algara MM, Augustynowicz M, et al. Lack of intracellular trehalose affects formation of Escherichia coli persister cells. Microbiol-Sgm. 2015; 161:786–96. https://doi.org/10.1099/mic.0.000012 WOS:000355366600010. PMID: 25500492

25. Murphy HN, Stewart GR, Mischenko VV, Apt AS, Harris R, McAlister MS, et al. The OtsAB pathway is essential for trehalose biosynthesis in *Mycobacterium tuberculosis*. J Biol Chem. 2005; 280(15):14524–9. Epub 2005/02/11. https://doi.org/10.1074/jbc.M414232200 PMID: 15703182.

26. Kalscheuer R, Syson K, Veeraraghavan U, Weinrick B, Biermann KE, Liu Z, et al. Self-poisoning of *Mycobacterium tuberculosis* by targeting GlgE in an alpha-glucan pathway. Nature Chemical Biology. 2010; 6(5):376–84. https://doi.org/10.1038/nchembio.340 WOS:000276823200017. PMID: 20305657

27. Piazza A, Zimaro T, Garavaglia BS, Ficarra FA, Thomas L, Marondedze C, et al. The dual nature of trehalose in citrus canker disease: a virulence factor for Xanthomonas citri subsp. citri and a trigger for plant defence responses. J Exp Bot. 2015; 66(9):2795–811. Epub 2015/03/17. https://doi.org/10.1093/jxb/erv095 PMID: 25770587; PubMed Central PMCID: PMC4986880.

28. Pazos-Rojas LA, Munoz-Arenas LC, Rodriguez-Andrade O, Lopez-Cruz LE, Lopez-Ortega O, Lopes-Olivares F, et al. Desiccation-induced viable but nonculturable state in Pseudomonas putida KT2440, a survival strategy. Plos One. 2019; 14(7). ARTN e0219554 https://doi.org/10.1371/journal.pone.0219554 WOS:000484971300010

29. De Smet KAL, Weston A, Brown IN, Young DB, Robertson BD. Three pathways for trehalose biosynthesis in mycobacteria. Microbiology. 2000; 146(1):199–208. https://doi.org/10.1099/00221287-146-1-199 PMID: 10658666

30. Giaever HM, Styrvold OB, Kaasen I, Strom AR. Biochemical and genetic characterization of osmoregulatory trehalose synthesis in *Escherichia coli*. Journal of Bacteriology. 1988; 170(6):2841–9. Epub 1988/06/01. https://doi.org/10.1128/jb.170.6.2841-2849.1988 PMID: 3131312; PubMed Central PMCID: PMC211211.

31. Wang TF, Jia SR, Dai K, Liu HJ, Wang RM. Cloning and expression of a trehalose synthase from Pseudomonas putida KT2440 for the scale-up production of trehalose from maltose. Canadian journal of microbiology. 2014; 60(9):599–604. https://doi.org/10.1139/cjm-2014-0330 WOS:000341919200006. PMID: 25204684

32. Miah F, Koliwer-Brandl H, Rejzek M, Field Robert A, Kalscheuer R, Bornemann S. Flux through Trehalose Synthase Flows from Trehalose to the Alpha Anomer of Maltose in Mycobacteria. Chemistry & biology. 2013; 20(4):487–93. https://doi.org/10.1016/j.chembiol.2013.02.014 PMC3918855. PMID: 23601637

33. Maruta K, Nakada T, Kubota M, Chaen H, Sugimoto T, Kurimoto M, et al. Formation of trehalose from maltooligosaccharides by a novel enzymatic system. Bioscience, Biotechnology, and Biochemistry. 1995; 59(10):1829–34. https://doi.org/10.1271/bbb.59.1829 PMID: 8534970

34. Avonce N, Mendoza-Vargas A, Morett E, Iturriaga G. Insights on the evolution of trehalose biosynthesis. BMC Evolutionary Biology. 2006; 6:109–. https://doi.org/10.1186/1471-2148-6-109 PMID: 17178000.

35. Edstrom RD. Structure of a low molecular weight form of glycogen isolated from the liver in a case of glycogen storage disease. J Biol Chem. 1972; 247(5):1360–7. Epub 1972/03/10. PMID: 4334997.

36. Sambou T, Dinadayala P, Stadthagen G, Barilone N, Bordat Y, Constant P, et al. Capsular glucan and intracellular glycogen of *Mycobacterium tuberculosis*: biosynthesis and impact on the persistence in mice. Molecular Microbiology. 2008; 70(3):762–74. https://doi.org/10.1111/j.1365-2958.2008.06445.x PMID: 18808383

37. Koliwer-Brandl H, Syson K, van de Weerd R, Chandra G, Appelmelk B, Alber M, et al. Metabolic network for the biosynthesis of intra- and extracellular α-glucans required for virulence of *Mycobacterium tuberculosis*. PLOS Pathogens. 2016; 12(8):e1005768. https://doi.org/10.1371/journal.ppat.1005768 PMID: 27513637

38. Preiss J. Bacterial glycogen synthesis and its regulation. Annual review of microbiology. 1984; 38:419–58. Epub 1984/01/01. https://doi.org/10.1146/annurev.mi.38.100184.002223 PMID: 6093684.

39. Espada J. Enzymic Synthesis of Adenosine Diphosphate Glucose from Glucose 1-Phosphate and Adenosine Triphosphate. Journal of Biological Chemistry. 1962; 237(12):3577–81.

40. Baecker PA, Furlong CE, Preiss J. Biosynthesis of bacterial glycogen. Primary structure of *Escherichia coli* ADP-glucose synthetase as deduced from the nucleotide sequence of the *glgC* gene. Journal of Biological Chemistry. 1983; 258(8):5084–8.

41. Fox J, Kawaguchi K, Greenberg E, Preiss J. Biosynthesis of bacterial glycogen. Purification and properties of the *Escherichia coli* B ADPglucose:1,4-alpha-D-glucan 4-alpha-glucosyltransferase. Biochemistry. 1976; 15(4):849–57. Epub 1976/02/24. https://doi.org/10.1021/bi00649a019 PMID: 2288.

42. Kumar A, Larsen CE, Preiss J. Biosynthesis of bacterial glycogen. Primary structure of *Escherichia coli* ADP-glucose:alpha-1,4-glucan, 4-glucosyltransferase as deduced from the nucleotide sequence of the *glgA* gene. J Biol Chem. 1986; 261(34):16256–9. Epub 1986/12/05. PMID: 3097003.

43. Larner J. The action of branching enzymes on outer chains of glycogen. J Biol Chem. 1953; 202(2):491–503. Epub 1953/06/01. PMID: 13061474.

44. Abad MC, Binderup K, Rios-Steiner J, Arni RK, Preiss J, Geiger JH. The X-ray crystallographic structure of *Escherichia coli* branching enzyme. J Biol Chem. 2002; 277(44):42164–70. Epub 2002/08/28. https://doi.org/10.1074/jbc.M205746200 PMID: 12196524.

45. Dauvillee D, Kinderf IS, Li Z, Kosar-Hashemi B, Samuel MS, Rampling L, et al. Role of the *Escherichia coli glgX* gene in glycogen metabolism. J Bacteriol. 2005; 187(4):1465–73. Epub 2005/02/03. https://doi.org/10.1128/JB.187.4.1465-1473.2005 PMID: 15687211; PubMed Central PMCID: PMC545640.

46. Alonso-Casajús N, Dauvillée D, Viale AM, Muñoz FJ, Baroja-Fernández E, Morán-Zorzano MT, et al. Glycogen Phosphorylase, the Product of the *glgP* Gene, Catalyzes Glycogen Breakdown by Removing Glucose Units from the Nonreducing Ends in *Escherichia coli*. Journal of Bacteriology. 2006; 188(14):5266–72. https://doi.org/10.1128/JB.01566-05 PMC1539952. PMID: 16816199

47. Elbein AD, Pastuszak I, Tackett AJ, Wilson T, Pan YT. Last step in the conversion of trehalose to glycogen: a mycobacterial enzyme that transfers maltose from maltose 1-phosphate to glycogen. J Biol Chem. 2010; 285(13):9803–12. Epub 2010/02/02. https://doi.org/10.1074/jbc.M109.033944 PMID: 20118231; PubMed Central PMCID: PMC2843229.

48. Chandra G, Chater KF, Bornemann S. Unexpected and widespread connections between bacterial glycogen and trehalose metabolism. Microbiology. 2011; 157(Pt 6):1565–72. Epub 2011/04/09. https://doi.org/10.1099/mic.0.044263-0 PMID: 21474533.

49. Freeman BC, Chen C, Beattie GA. Identification of the trehalose biosynthetic loci of *Pseudomonas syringae* and their contribution to fitness in the phyllosphere. Environmental Microbiology. 2010; 12(6):1486–97. Epub 2010/03/03. https://doi.org/10.1111/j.1462-2920.2010.02171.x PMID: 20192963.

50. Djonović S, Urbach JM, Drenkard E, Bush J, Feinbaum R, Ausubel JL, et al. Trehalose biosynthesis promotes *Pseudomonas aeruginosa* pathogenicity in plants. PLoS Pathogens. 2013; 9(3):e1003217. https://doi.org/10.1371/journal.ppat.1003217 PMID: 23505373

51. Harty CE, Martins D, Doing G, Mould DL, Clay ME, Occhipinti P, et al. Ethanol Stimulates Trehalose Production through a SpoT-DksA-AlgU-Dependent Pathway in Pseudomonas aeruginosa. Journal of Bacteriology. 2019; 201(12). doi:ARTN e00794 https://doi.org/10.1128/JB.00794-18 WOS:000468610700012. PMID: 30936375

52. Behrends V, Ryall B, Wang XZ, Bundy JG, Williams HD. Metabolic profiling of Pseudomonas aeruginosa demonstrates that the anti-sigma factor MucA modulates osmotic stress tolerance. Molecular bioSystems. 2010; 6(3):562–9. https://doi.org/10.1039/b918710c WOS:000274654400013. PMID: 20174684

53. Behrends V, Ryall B, Zlosnik JEA, Speert DP, Bundy JG, Williams HD. Metabolic adaptations of Pseudomonas aeruginosa during cystic fibrosis chronic lung infections. Environmental Microbiology. 2013; 15(2):398–408. https://doi.org/10.1111/j.1462-2920.2012.02840.x WOS:000314211100009. PMID: 22882524

54. Mao F, Dam P, Chou J, Olman V, Xu Y. DOOR: a database for prokaryotic operons. Nucleic Acids Res. 2009; 37(Database issue):D459–63. Epub 2008/11/08. https://doi.org/10.1093/nar/gkn757 PMID: 18988623; PubMed Central PMCID: PMC2686520.

55. Freeman BC, Chen C, Beattie GA. Identification of the trehalose biosynthetic loci of Pseudomonas syringae and their contribution to fitness in the phyllosphere. Environ Microbiol. 2010; 12(6):1486–97. https://doi.org/10.1111/j.1462-2920.2010.02171.x PMID: 20192963.

56. Winsor GL, Griffiths EJ, Lo R, Dhillon BK, Shay JA, Brinkman FS. Enhanced annotations and features for comparing thousands of Pseudomonas genomes in the Pseudomonas genome database. Nucleic Acids Res. 2016; 44(D1):D646–53. Epub 2015/11/19. https://doi.org/10.1093/nar/gkv1227 PMID: 26578582; PubMed Central PMCID: PMC4702867.

57. Syson K, Stevenson CEM, Rejzek M, Fairhurst SA, Nair A, Bruton CJ, et al. Structure of Streptomyces Maltosyltransferase GlgE, a Homologue of a Genetically Validated Anti-tuberculosis Target. Journal of Biological Chemistry. 2011; 286(44):38298–310. https://doi.org/10.1074/jbc.M111.279315 WOS:000296594200043. PMID: 21914799

58. Kartal O, Mahlow S, Skupin A, Ebenhoh O. Carbohydrate-active enzymes exemplify entropic principles in metabolism. Mol Syst Biol. 2011; 7:542. Epub 2011/10/27. https://doi.org/10.1038/msb.2011.76 PMID: 22027553; PubMed Central PMCID: PMC3261701.

59. Bailey JM, Whelan WJ. Physical properties of starch. I. Relationship between iodine stain and chain length. J Biol Chem. 1961; 236:969–73. Epub 1961/04/01. PMID: 13685959.

60. Rashid AM, Batey SFD, Syson K, Koliwer-Brandl H, Miah F, Barclay JE, et al. Assembly of alpha-Glucan by GlgE and GlgB in Mycobacteria and Streptomycetes. Biochemistry. 2016; 55(23):3270–84. https://doi.org/10.1021/acs.biochem.6b00209 WOS:000378016500012. PMID: 27221142

61. Holden PA. Biofilms in unsaturated environments. In: Doyle RJ, editor. Methods in Enzymology. 337: Academic Press; 2001. p. 125–43. https://doi.org/10.1016/s0076-6879(01)37011-8 PMID: 11398425

62. Van De Mortel M, Halverson LJ. Cell envelope components contributing to biofilm growth and survival of *Pseudomonas putida* in low-water-content habitats. Molecular Microbiology. 2004; 52(3):735–50. https://doi.org/10.1111/j.1365-2958.2004.04008.x PMID: 15101980

63. Manzanera M, García-Fontana C, Vílchez JI, Narváez-Reinaldo JJ, González-López J. Genome sequence of *Microbacterium* sp. Strain 3J1, a highly desiccation-tolerant bacterium that promotes plant growth. Genome Announcements. 2015; 3(4):e00713–15. https://doi.org/10.1128/genomeA.00713-15 PMC4551875. PMID: 26316631

64. Klähn S, Hagemann M. Compatible solute biosynthesis in cyanobacteria. Environmental Microbiology. 2011; 13(3):551–62. https://doi.org/10.1111/j.1462-2920.2010.02366.x PMID: 21054739

65. Yoshida T, Sakamoto T. Water-stress induced trehalose accumulation and control of trehalase in the cyanobacterium *Nostoc punctiforme* IAM M-15. The Journal of General and Applied Microbiology. 2009; 55(2):135–45. https://doi.org/10.2323/jgam.55.135 PMID: 19436130

66. Gulez G, Dechesne A, Workman CT, Smets BF. Transcriptome dynamics of *Pseudomonas putida* KT2440 under water stress. Appl Environ Microb. 2012; 78(3):676–83. Epub 2011/12/06. https://doi.org/10.1128/AEM.06150-11 PMID: 22138988; PubMed Central PMCID: PMC3264132.

67. Freeman BC, Chen C, Yu X, Nielsen L, Peterson K, Beattie GA. Physiological and transcriptional responses to osmotic stress of two *Pseudomonas syringae* strains that differ in their epiphytic fitness and osmotolerance. Journal of Bacteriology. 2013. https://doi.org/10.1128/JB.00787-13 PMID: 23955010

68. Preiss J. Biochemistry and Molecular Biology of Glycogen Synthesis in Bacteria and Mammals and Starch Synthesis in Plants. In: Liu H-W, Mander L, editors. Comprehensive Natural Products II. Oxford: Elsevier; 2010. p. 429–91.

69. Geurtsen J, Chedammi S, Mesters J, Cot M, Driessen NN, Sambou T, et al. Identification of Mycobacterial α-Glucan as a novel ligand for DC-SIGN: involvement of mycobacterial capsular polysaccharides in host immune modulation. The Journal of Immunology. 2009; 183(8):5221–31. https://doi.org/10.4049/jimmunol.0900768 PMID: 19783687

70. Stover CK, Pham XQ, Erwin AL, Mizoguchi SD, Warrener P, Hickey MJ, et al. Complete genome sequence of Pseudomonas aeruginosa PA01, an opportunistic pathogen. Nature. 2000; 406. https://doi.org/10.1038/35023079 PMID: 10984043

71. Buell CR, Joardar V, Lindeberg M, Selengut J, Paulsen IT, Gwinn ML, et al. The complete genome sequence of the *Arabidopsis* and tomato pathogen *Pseudomonas syringae* pv. *tomato* DC3000. Proc Natl Acad Sci U S A. 2003; 100(18):10181–6. Epub 2003/08/21. https://doi.org/10.1073/pnas.1731982100 PMID: 12928499; PubMed Central PMCID: PMC193536.

72. Quiles F, Polyakov P, Humbert F, Francius G. Production of extracellular glycogen by Pseudomonas fluorescens: spectroscopic evidence and conformational analysis by biomolecular recognition. Biomacromolecules. 2012; 13(7):2118–27. Epub 2012/06/13. https://doi.org/10.1021/bm300497c PMID: 22686500.

73. Aspedon A, Palmer K, Whiteley M. Microarray analysis of the osmotic stress response in Pseudomonas aeruginosa. J Bacteriol. 2006; 188. https://doi.org/10.1128/JB.188.7.2721-2725.2006 PMID: 16547062

74. Miller JH. Experiments in molecular genetics: Cold Spring Harbor Laboratory; 1972.

75. Sambrook J, Fritsch EF, Maniatis T. Molecular Cloning: A Laboratory Manual: Cold Spring Harbor Laboratory; 1989.

76. Voisard C, Bull CT, Keel C, Laville J, Maurhofer M, Schnider U, et al. Biocontrol of Root Diseases by *Pseudomonas fluorescens* CHA0: Current Concepts and Experimental Approaches. Molecular Ecology of Rhizosphere Microorganisms: Wiley-VCH Verlag GmbH; 1994. p. 67–89. https://doi.org/10.1016/0167-5273(94)90206-2 PMID: 8181884

77. Choi KH, Kumar A, Schweizer HP. A 10-min method for preparation of highly electrocompetent *Pseudomonas aeruginosa* cells: application for DNA fragment transfer between chromosomes and plasmid transformation. J Microbiol Methods. 2006; 64(3):391–7. Epub 2005/07/01. https://doi.org/10.1016/j.mimet.2005.06.001 PMID: 15987659.

78. Malone JG, Jaeger T, Spangler C, Ritz D, Spang A, Arrieumerlou C, et al. YfiBNR mediates cyclic di-GMP dependent small colony variant formation and persistence in Pseudomonas aeruginosa. PLoS Pathog. 2010; 6(3):e1000804. https://doi.org/10.1371/journal.ppat.1000804 PMID: 20300602.

79. Heeb S, Itoh Y, Nishijyo T, Schnider U, Keel C, Wade J, et al. Small, stable shuttle vectors based on the minimal pVS1 replicon for use in gram-negative, plant-associated bacteria. Molecular plant-microbe interactions: MPMI. 2000; 13(2):232–7. https://doi.org/10.1094/MPMI.2000.13.2.232 PMID: 10659714.

80. Choi K-H, Gaynor JB, White KG, Lopez C, Bosio CM, Karkhoff-Schweizer RR, et al. A Tn7-based broad-range bacterial cloning and expression system. Nature methods. 2005; 2:443. https://doi.org/10.1038/nmeth765 https://www.nature.com/articles/nmeth765#supplementary-information. PMID: 15908923

81. Studier FW. Protein production by auto-induction in high density shaking cultures. Protein Expr Purif. 2005; 41(1):207–34. Epub 2005/05/26. https://doi.org/10.1016/j.pep.2005.01.016 PMID: 15915565.

82. Usui T, Yokoyama M, Yamaoka N, Matsuda K, Tuzimura K, Sugiyama H, et al. Proton magnetic resonance spectra of D-gluco-oligosaccharides and D-glucans. Carbohydrate research. 1974; 33(1):105–16. doi:http://dx.doi.org/10.1016/S0008-6215(00)82944-4

83. De Goffau MC, Yang X, Van Dijl JM, Harmsen HJM. Bacterial pleomorphism and competition in a relative humidity gradient. Environmental Microbiology. 2009; 11(4):809–22. https://doi.org/10.1111/j.1462-2920.2008.01802.x PMID: 19040453